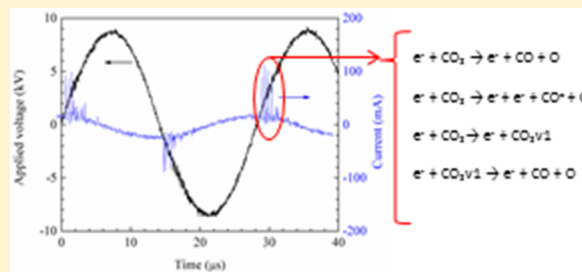


Influence of Vibrational States on CO₂ Splitting by Dielectric Barrier Discharges

Robby Aerts,* Tom Martens, and Annemie Bogaerts

Department of Chemistry, PLASMANT Research Group, University of Antwerp, Universiteitsplein 1, B-2610 Wilrijk-Antwerp, Belgium

ABSTRACT: In this paper, the splitting of CO₂ in a pulsed plasma system, such as a dielectric barrier discharge (DBD), is evaluated from a chemical point of view by means of numerical modeling. For this purpose, a chemical reaction set of CO₂ in an atmospheric pressure plasma is developed, including the vibrational states of CO₂, O₂, and CO. The simulated pulses are matched to the conditions of a filament (or microdischarge) and repeated with intervals of 1 μs. The influence of vibrationally excited CO₂ as well as other neutral species, ions, and electrons on the CO₂ splitting is discussed. Our calculations predict that the electrons have the largest contribution to the CO₂ splitting at the conditions under study, by electron impact dissociation. The contribution of vibrationally excited CO₂ levels in the splitting of CO₂ is found to be 6.4%, when only considering one microdischarge pulse and its afterglow, but it can be much higher for consecutive discharge pulses, as is typical for a filamentary DBD, when the interpulse time is short enough and accumulation effects in the vibrationally excited CO₂ densities can occur.



1. INTRODUCTION

In recent years, there has been a growing interest in the plasma assisted conversion of greenhouse gases, such as CH₄ and CO₂, into compounds such as methanol (CH₃OH) or syngas (CO/H₂) that are of interest as building blocks for the chemical industry or that can be used as a fuel.^{1–3} Plasmas, or gas discharges, are of interest for two major reasons. First, such discharges are known to activate the molecules vibrationally and electronically so that the chemical conversion is stimulated. Second, the generation of electricity from renewable sources such as wind and solar cells is fluctuating, which makes it often difficult to match the supply of this electricity with the demand. As a consequence, often a surplus of electricity is generated, which is difficult to store. This surplus of electricity could then be used in gas discharges to convert greenhouse gases into value-added chemicals. Alternatively, this surplus of energy can also be used for the production of hydrogen.⁴ However, hydrogen is a very volatile gas, which makes it difficult to store and to transport, in comparison with a liquid such as methanol.

In order to optimize the plasma-based gas conversion, thorough insight into the plasma chemistry is needed. The present paper concerns the splitting of CO₂ in an atmospheric pressure plasma, because CO₂ is one of the most important greenhouse gases. The use of CO₂ as a feedstock gas is recognized as a very important scientific challenge for the present and the future. Indeed, in certain processes in chemical industry it is available in an almost pure form as a waste gas, and using highly advanced adsorbing techniques it can be extracted from the air.⁵ However, due to its highly oxidized character and very low reactivity it is not straightforward to be used as a feedstock gas.

To overcome the inert character of CO₂, gas discharges can be very useful, as the electrons can activate the molecules.

More specifically, the vibrational excitations can stimulate the dissociation and the electronic excitations can stimulate ionization. The discharge under study in this work is an atmospheric pressure dielectric barrier discharge (DBD). It consists of two electrodes of which at least one electrode is electrically insulated. This electrical insulation or dielectric prevents the discharge from transforming into an arc discharge which would damage the electrodes. Operating at atmospheric pressure has the great advantage that vacuum equipment can be avoided and that in-line processing is possible.³

As mentioned above, in order to use CO₂ as a feedstock gas, it has to be split into O₂ and CO, which is a valuable feedstock gas for the chemical industry. Although the atomic and molecular plasma chemistry can be very complex, the splitting of CO₂ can be summarized as follows:



Thermodynamically, this reaction requires 283 kJ/mol or 2.94 eV/molecule at 400 K and atmospheric pressure.

In order to obtain a detailed description of the CO₂ splitting, a reaction set is constructed which contains the vibrational and electronic excitations of the CO₂, CO, and O₂ molecules, because previous publications on pure CO₂ splitting by plasma showed that only these species were important.^{2,6–8} Previous studies which included these excited states usually only described the formation and quenching of these states but not their further role in the plasma chemistry,⁹ whereas it is known that up to 97% of the discharge power for a low-temperature plasma can go to the

Received: July 30, 2012

Revised: September 17, 2012

Published: October 19, 2012

vibrational excitation in a molecular plasma.^{10,11} Therefore, in the present work we include the influence of the vibrationally and electronically excited species on the ongoing chemistry. The experimental setup under study is a cylindrical DBD, inspired by the series of research performed at Moscow State University between 1960 and 1970.^{12–20} In these papers, a classic silent discharge for ozone production was applied for organic gas conversion.^{21,22} The starting point in our research is the same; however, in future work, we would like to evaluate the effectiveness of plasma catalysis for this setup. The specific cylindrical DBD under study in this work was presented in Paulussen et al.³ The outer electrode is powered and is formed by sputtering chromium over a length of 90 mm on the outside of an alumina tube with an external diameter of 30 mm and an inner diameter of 26 mm. The inner electrode is grounded. It is a stainless steel tube with an outer diameter of 22 mm. Therefore, the discharge gap is 2 mm. A voltage of typically about 20 kV_{peak-to-peak} is applied at a frequency of 50 kHz. In the present work the averaged applied power will always be 150 W. More details on the setup were previously reported by Paulussen et al.³

In the next section, we will present the physical model that is used, as well as the chemical reaction set. In the Results and Discussion section, first the influence of the electrons on the chemical splitting mechanism in CO₂ for a single power pulse will be investigated. Second, we will study the vibrational chemistry for a single power pulse and its afterglow, as well as a series of pulses. Third we will investigate the behavior of the various ions and neutral species, both for a single power pulse and a series of pulses, and finally, the contribution of the different species to the splitting of CO₂ will be evaluated.

2. DESCRIPTION OF THE SIMULATIONS

2.1. Description of the Physical Model. The simulations in this work are performed using the numerical model Global_kin developed by Dorai and Kushner.^{23,24} We used two basic modules of this model: the Boltzmann equation module and a zero-dimensional plasma chemistry module. First, a reaction mechanism is defined (see below). Next, the Boltzmann equation module calculates the values of the reaction rate coefficients for the electron impact reactions, based on the collision cross sections, and depending on the electron energy, and subsequently look-up tables with these rate coefficients as a function of electron energy (or electron temperature) are created. These coefficients will then be used as input in the chemistry module to calculate the source terms for the electron impact gas phase reactions, leading to production and loss of the various plasma species. The rate coefficients for the other gas phase reactions, i.e., between heavy plasma species, are adopted from literature, as illustrated in the Appendix. Hence, the time-evolution in number density of the various plasma species is calculated from

$$\frac{dn_i}{dt} = \sum_j [(a_{ij}^R - a_{ij}^L)k_j \prod_l n_l^L] \quad (\text{E1})$$

where n_i is the density of species i , a_{ij}^R and a_{ij}^L are the right-hand side and left-hand side stoichiometric coefficients of species i in reaction j , k_j is the reaction rate coefficient, and n_l^L is the density of the l th species in the left-hand side of reaction j . Note that no transport is included in this chemistry module. Indeed, the plasma reactor is considered as a batch reactor, with a uniform concentration of species over the entire reactor volume.

The electron induced reactions depend on electron temperature, which changes, on one hand, due to Joule heating from the

applied power, and on the other hand, due to the energy lost in collisions. The electron temperature is calculated from

$$\frac{d}{dt} \left(\frac{3}{2} n_e k_B T_e \right) = \vec{j} \cdot \vec{E} - \sum_i \frac{3}{2} n_e \nu_{m,i} \left(\frac{2m_e}{M_i} \right) k_B (T_e - T_i) + \sum_l n_e k_l N_l \Delta \varepsilon_l \quad (\text{E2})$$

where n_e is the electron density, k_B is Boltzmann's constant, T_e is the electron temperature, \vec{j} and \vec{E} are the current density and the electric field in the discharge, $\nu_{m,i}$ is the electron momentum transfer collision frequency with species i , m_e is the electron mass, and M_i and T_i are the mass and temperature of species i . Finally, k_l is the reaction rate coefficient for the l th electron impact process, N_l is the density of the gas phase collision partner, and $\Delta \varepsilon_l$ is the corresponding change in the electron energy (hence negative for energy loss). To summarize, the first term expresses the Joule heating, whereas the second and third terms represent the energy loss due to elastic and inelastic collisions, respectively. Since the model is zero-dimensional, the product of current density with electric field is not used here to calculate the Joule heating, but instead, the ratio of the applied power to the plasma volume is used, which is equivalent.

The chemistry module is called every time step but the Boltzmann module is only called when the background gas density has changed significantly. Indeed, it is not necessary to call this Boltzmann module in every time step. This will be specified in more detail in the Results and Discussion section, since it differs from case to case. More details on the model can be found in the papers by Dorai and Kushner.^{23,24}

In this work the Global_kin model was extended with a reaction analysis module so that automatically an overview is printed of all absolute contributions of the relevant reactions to the production and loss of every species. For the absolute contributions, eq R1 is used. Next to the absolute contributions, also the relative contributions of the relevant reactions to the production and loss of a species are calculated from

$$\gamma_{ij} = ((a_{ij}^R - a_{ij}^L)k_j \prod_l n_l^L) / \left(\frac{dn_i}{dt} \right)_{\text{prod/loss}} \quad (\text{E3})$$

where γ_{ij} is the relative contribution of reaction j to the production or loss of species i , which is always evaluated versus the total dn_{ij}/dt production or loss. All other parameters have the same meaning as in eq E1.

It should be mentioned that gas heating was not calculated explicitly in the model, but a gas temperature of 400 K was assumed. We know from experiments that the bulk gas temperature does not rise significantly, i.e., the gas at the outlet is still more or less at room temperature. There could be local heating during one single microdischarge. However, we expect that the influence on the chemistry is quite small, as it does not influence the electron impact reactions, which are found to be the most important reactions during the microdischarge pulse (see below).

2.2. Description of the Chemistry. The species included in the model are presented in Table 1, and an overview of all chemical reactions considered in the model is given in the Appendix. Eight neutral species (i.e., ground state molecules and radicals, related to CO₂ and O₂) are taken into account, as well as 11 different positive ions and 6 different negative ions. Moreover, several excited levels of CO₂, CO, and O₂ are considered, as outlined in Table 2. These levels have been grouped into effective levels, in order to limit the number of chemical reactions in the model. Indeed, the number of reactions can quickly increase if

Table 1. Overview of the Ground-State Species Included in the Model

neutrals and radicals	ions
CO ₂ , CO, C ₂ O	CO ₂ ⁺ , CO ₄ ⁺ , CO ⁺ , C ₂ O ₂ ⁺
C, C ₂	C ₂ O ₃ ⁺ , C ₂ O ₄ ⁺ , C ⁺ , C ₂ ⁺
	CO ₃ ⁻ , CO ₄ ⁻
O ₂ , O ₃ , O	O ₂ ⁺ , O ⁺ , O ₄ ⁺
	O ⁻ , O ₂ ⁻ , O ₃ ⁻ , O ₄ ⁻

Table 2. Overview of Excited Species Included in the Model

ground state	notation in the model	described excited state(s)
CO ₂	CO ₂ v1	(010)
	CO ₂ v2	(100), (020)
	CO ₂ v3	(001)
	CO ₂ v4	(n00), (0n0)
	CO ₂ e1	CO ₂ (¹ Π _g)
	CO ₂ e2	CO ₂ (¹ Δ _u)
CO	COv1	sum of vibrations
	COe1	CO(A ³ Π)
	COe2	CO(A ¹ Π)
	COe3	CO(A ³ Σ), CO(D ³ Δ), CO(E ³ Σ), CO(B ³ Σ)
	COe4	CO(C ¹ Σ), CO(E ¹ Π), CO(B ¹ Σ), CO(I ¹ Σ), CO(D ¹ Δ)
O ₂	O ₂ v1	(n _v = 1,2)
	O ₂ v2	(n _v = 3,4)
	O ₂ v3	(n _v = 5,6)
	O ₂ e1	O ₂ (a ¹ Δ) and O ₂ (b ¹ Σ)
	O ₂ e2	O ₂ (B ³ Σ) and higher triplets

every excited species can react in a similar way as its ground state. This becomes more important in a later stage when time consumption becomes an issue, i.e., when this chemistry will be used to simulate full geometries in two- or three-dimensional models.

After critical evaluation of the available cross sections of CO₂, CO and O₂, several groups of levels were defined (see Table 2).^{25–30} The different vibrational levels of CO₂ have been grouped in four different levels, denoted as CO₂v1, CO₂v2, CO₂v3 and CO₂v4. CO₂v1 represents the first bending mode (010), CO₂v2 is the sum of the first symmetric stretch (100) and the second bending mode (020), CO₂v3 denotes the first asymmetric stretch mode (001), and finally, CO₂v4 represents the sum of the higher symmetric stretch (n00) and bending (0n0) modes. It should be clear that, by combining these higher vibrational levels into one “effective” vibrational level, it is not possible to describe the VV transfers to higher vibrational levels, as mentioned by Fridman.^{10,11} However, for high values of reduced electric field (i.e., higher than 100 Td) as is the case in DBDs, the VV transfers to higher levels will not be of such a great importance as for example in a microwave discharge, where most of the energy is transferred to the vibrationally excited states.^{10,11} Hence, although the CO₂ vibrational kinetics is in reality still much more complicated, we believe that this approximation is justified for the present study, and that the trends of the influence of vibrational levels can be qualitatively predicted for a DBD. The electronic excitation of CO₂ is described using two levels, i.e., CO₂(¹Π_g) (denoted as CO₂e1) and CO₂(¹Δ_u) (symbolized as CO₂e2).

For CO, all vibrational excitation is described using one mode, i.e., COv1, at a threshold of 1.01 eV. The electronic excitations have been grouped in four different levels. COe1 describes the excited level CO(A³Π), COe2 stands for the excited level CO(A¹Π), COe3 is the sum of the triplet levels CO(A³Σ),

CO(D³Δ), CO(E³Σ), and CO(B³Σ), and finally, COe4 describes the sum of the singlet levels CO(C¹Σ), CO(E¹Π), CO(B¹Σ), CO(I¹Σ), and CO(D¹Δ).

O₂ is described using three vibrational states: O₂v1 denotes the first and second vibrational level. O₂v2 symbolizes the third and fourth vibrational level and O₂v3 stands for the fifth and sixth vibrational level. The electronic excitations are grouped into two states: O₂e1 groups the singlet states O₂(a¹Δ) and O₂(b¹Σ), while O₂e2 is the sum of O₂(B³Σ) and the higher triplet states.

These excited states have the same chemistry as their ground state levels (see below), except that the vibrationally excited states typically have a stimulated dissociation and the electronically excited states can have a stimulated ionization, i.e. the activation barriers of ionization and dissociation are lowered as a consequence of the higher energy level of the excited reactants. Indeed, because the energy requirement to dissociate a vibrationally excited molecule is lower than for a ground state molecule, the threshold energy for the electron induced reactions is lowered with the same amount as the vibrational excitation energy.

The production of these vibrationally and electronically excited levels is by electron impact excitation, as outlined in the Appendix. Furthermore, we consider 3 types of loss processes for the vibrationally excited molecules. The first one is by electron impact reactions (see the Appendix), for which the corresponding cross section is shifted on the energy scale toward a lower energy. The second loss process is by VT and VV transfers with the ground state species CO₂, CO, and O₂, for which the rate coefficients were adopted from literature and recalculated for a temperature of 400 K.^{31,32}

Finally, the third type of loss process is the interaction of heavy particles (i.e., ions and neutrals) with vibrationally excited states, which causes a bond break in the excited molecule. This process was taken into account by adopting the theory described by the Fridman–Macheret α -Model.^{10,11} This theory uses an Arrhenius expression for the reaction rate coefficient

$$k_{\text{R}}(E_{\text{v}}, T_{\text{g}}) = k_{\text{R}0} \exp\left(-\frac{E_{\text{a}} - \alpha E_{\text{v}}}{T_{\text{g}}}\right) \theta(E_{\text{a}} - \alpha E_{\text{v}}) \quad (\text{E4})$$

In this equation E_{a} is the activation energy of an elementary chemical reaction and E_{v} is the vibrational energy. The coefficient α is the efficiency of the excitation energy use in overcoming the activation barrier, $k_{\text{R}0}$ is the pre-exponential factor and $\theta(a - b)$ is the so-called Heaviside function, which is zero when $b > a$ and it is 1 when $a \geq b$. The values for α were taken from Fridman and were only considered if there is a bond break in the vibrationally excited molecule.^{10,11} For exothermic reactions, $\alpha = 0.3$ was used, whereas for thermo-neutral reactions, $\alpha = 0.45$ is used and for one exothermic double exchange (i.e., reaction (74) of Table 6 in the Appendix) $\alpha = 0.2$ was used.

A similar procedure as described above is also used for the electronically excited species. The cross sections for electron induced ionizations are shifted on the energy scale to a lower energy with the same amount as the electronic excitation energy. For the interactions between heavy particles this effect is only considered for charge exchange reactions, because in such reaction ionization occurs in the electronically excited species. Classically, for such a reaction the collision cross section has a reverse proportionality with the square of the ionization potential and the reaction rate coefficient is proportional to the collision cross section.¹⁰ Therefore, the stimulation of charge exchange with electronically excited species was implemented as

$$k_{\text{R}} = k_{\text{R}0}((E_{\text{I}})^2 / (E_{\text{E}})^2) \quad (\text{E5})$$

where k_{RO} is the original reaction rate coefficient, E_I is the ionization potential of the excited species and E_E is the electronic excitation threshold energy. Reaction 132 (see Table 8 of the Appendix) is a different type of reaction, but it is known that for this reaction the increase in reaction rate is also significant.³⁴ Therefore, to describe this reaction with O_2e1 and O_2e2 , we used the value $k = 3 \times 10^{-10} \text{ cm}^3 \text{ s}^{-1}$, as suggested by Kosygi and co-workers.³⁴ Finally, the rate coefficients for the relaxation of the electronic excited states were estimated according to their expected lifetime and the report by Surzhikov.³²

The resulting reaction chemistry consists of 42 chemical species (i.e., the species presented in Table 1 and Table 2, as well as the electrons), who engage in 501 chemical reactions. The chemical reactions of the ground state species, together with the VV and VT transfers adopted from literature, are tabulated in the Appendix, as well as the corresponding rate coefficients and the references where these data are adopted from. As mentioned above, the same reactions are also included for the electronic and vibrationally excited species, but with modified rate coefficients, as explained above.

3. RESULTS AND DISCUSSION

3.1. Validation of the Model. As our model is developed and applied here to study the plasma chemistry in one pulse (microdischarge) and afterglow, or five consecutive pulses in the microsecond time-scale (see below), comparison with experimental data to validate the model at this stage is extremely difficult. Therefore, initial validation of our model is performed by comparison with the validated modeling results from Cenian and co-workers.³⁵ The research of Cenian et al. concerned a pure CO_2 discharge, operating at 30 Torr and a temperature of 400 K, with an applied potential difference of 200 V between the electrodes and a current density of 7.5 A/cm^2 , which leads to a power density of 1.5 kW/cm^2 . To compare our model results with the work by Cenian, the same power density was implemented in our simulations. The fractional densities calculated by our model are plotted in Figure 1, together with the results from Cenian and

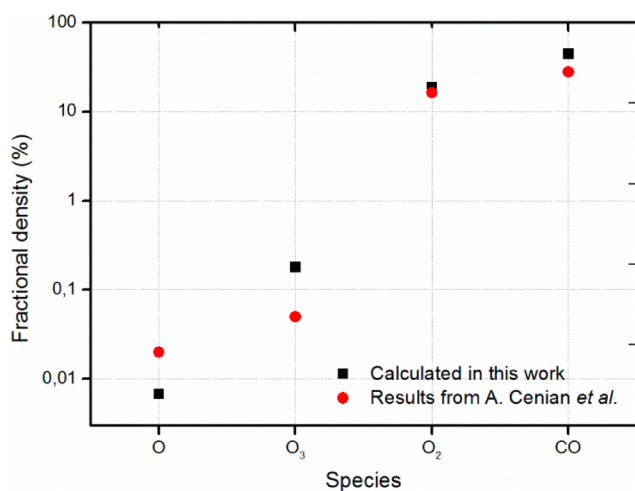


Figure 1. Calculated fractional densities of CO_2 conversion products, at 30 Torr, 400 K, and a power input of 1.5 kW/cm^2 , obtained in this work, in comparison with the results from Cenian and co-workers.³⁵

co-workers.³⁵ The calculated fractional CO and O_2 densities are nearly the same as found by Cenian. CO is calculated to be present for about 30% in the discharge and O_2 for about 17%. O_3 has a calculated fractional density of 0.05% in the discharge, which is

slightly lower than the results of Cenian, while the calculated fractional density of the O atoms (i.e., 0.02%) is somewhat higher. However, the obtained densities for O_3 and O are still in the same order of magnitude as the results obtained by Cenian. These differences are not unexpected since the chemical reaction set is considerably different. Nevertheless, the agreement for the densities of the most important species, i.e., CO and O_2 , is very good, which provides us at least with some validation of our model.

3.2. Description of the Power Deposition in the Model.

To match the conditions of a dielectric barrier discharge (DBD), some characteristic discharge pulses were implemented in the model. Indeed, experimentally these discharges are filamentary, meaning that breakdown occurs at different positions at the same time.^{10,33} Such effects can, however, not be included in a zero-dimensional simulation. Nevertheless, we know that a typical voltage/current waveform of a DBD in a reactive gas shows nanosecond pulses which are repeated in the (sub-) microsecond region.³ Therefore, for simplicity, we implemented a triangular 30 ns discharge pulse, every microsecond, based on the fact that in one-half period breakdown occurs which results in nanosecond fluctuations for a range of over a couple of microseconds.^{3,36} Actually, we do not know how many pulses every molecule passes in real time; therefore the purpose of this simulation is to evaluate the effect of a number of microdischarges as a case study for long time scale simulations.

Figure 2 presents the calculated electron density and electron temperature, as well as the applied power, as a function of time

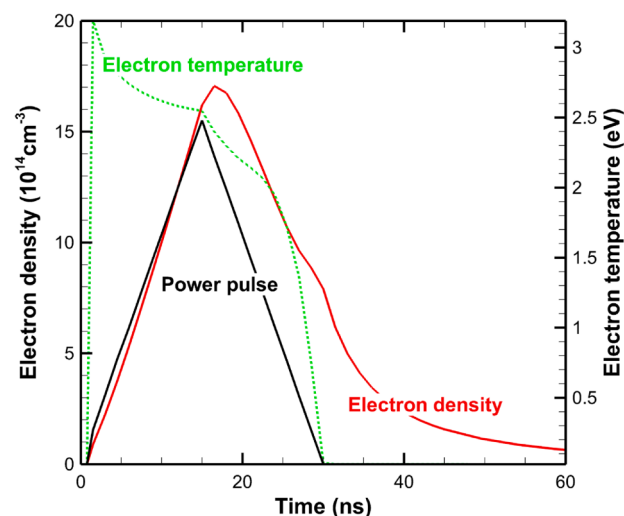


Figure 2. Calculated electron temperature (dashed green line; right y axis) and electron density (solid red line; left y axis) as a function of time during a single-pulse discharge and its afterglow. The applied power pulse is indicated by the solid black line (not shown on y axis).

for one pulse. In order to match the conditions of our pulse as close as possible to a single microdischarge, the power of the pulse was set to a maximum value of $8.0 \times 10^7 \text{ W}$ at 15 ns, which results in a calculated maximum electron temperature of 2.6 eV and a maximum electron density of $1.65 \times 10^{15} \text{ cm}^{-3}$, as shown in Figure 2. Indeed, these values of electron temperature and electron density match typical values reported in literature for microdischarges.^{10,37} As is clear from Figure 2, the largest change in densities takes place when the pulse reaches its maximum at 15 ns; therefore, the Boltzmann equation module will be called at the beginning and in the middle of every pulse. The calculation results presented below are all obtained for the pulse described

above, with its corresponding electron temperature and electron density profiles shown in Figure 2, and for an initial CO_2 density of $1.8 \times 10^{19} \text{ cm}^{-3}$.

3.3. Energy Transfer from Electrons to Different Channels of CO_2 Excitation, Ionization, and Dissociation.

Before looking in detail at the plasma chemistry of the CO_2 splitting, we wish to obtain first some insight in how the electron energy is transferred to different channels of excitation, ionization, or dissociation of the CO_2 molecule. Indeed, the driving force behind plasma processing must be found in the electrons, which contribute in many electron impact reactions, especially for stable molecules as CO_2 . To distinguish between the different energy loss processes of electrons, Figure 3 illustrates the fractional

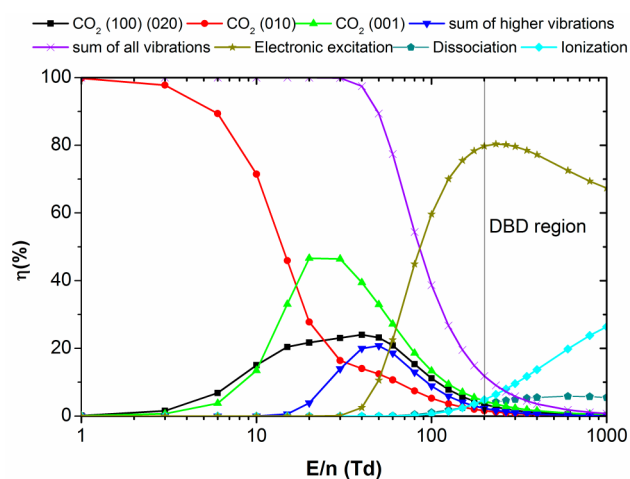


Figure 3. Fractions of electron energy transferred to different channels of excitation as well as ionization and dissociation of CO_2 , as a function of the reduced electric field (E/n), as calculated from the corresponding cross sections of the electron impact reactions. The E/n region characteristic for dielectric barrier discharges is indicated by “DBD region”. The electron impact dissociation reaction of CO_2 through electron impact excitation, followed by dissociation, is mentioned in the figure as “dissociation”. The sum of electron impact electronic excitation reactions of CO_2 which form excited levels without dissociation are mentioned as “Electronic excitation”.

energy transferred from electrons to different channels of CO_2 excitation, ionization and dissociation, as a function of the reduced electric field (E/n) in a discharge. This plot is constructed based on the cross sections of the corresponding electron impact reactions, as a function of electron energy, which is calculated for the different values of E/n , shown in the x axis.

Fridman and co-workers stated that for gas discharges with an electron temperature around 1–2 eV, or a reduced electric field (E/n) of about 20–40 Td, up to 97% of the total nonthermal discharge energy can be transferred from plasma electrons to vibrational excitation of CO_2 molecules.^{10,11,38} This is indeed indicated by the calculated “sum of all vibrations” curve in Figure 3. A similar plot was also presented in the book of Fridman.¹⁰ However, the electron temperature in a DBD is about 2–3 eV. These values correspond to E/n values of about 200 Td or higher. This region is indicated as “DBD region” in the figure. It is clear that in this region at maximum only 12% of the energy is transferred to the vibrational states, whereas $\sim 79\%$ goes to electronic excited states, while $\sim 4\%$ and $\sim 5\%$ are transferred to dissociation and ionization of CO_2 , respectively, with a further increasing contribution at rising E/n . This suggests that vibrationally excited states

might not be so important for CO_2 splitting in a DBD as it would be in other types of discharges that are characterized by lower values of E/n , such as microwave discharges.^{10,39} Fridman indeed investigated different discharges for CO_2 splitting and concluded that higher pressures and lower values of reduced electric field make the vibrational excitation mechanism more favorable than the electronic excitation mechanism, explaining the higher energy efficiency of these type of discharges (e.g., microwave, gliding arc discharges).^{10,11,39–42} In the next section we will try to elucidate the role of the various plasma processes and plasma species, present in a DBD, on the actual dissociation of CO_2 .

3.4. Evaluation of the Important Splitting Reactions and Plasma Species in a DBD. The actual splitting of CO_2 can be reached upon electron impact from the ground state or the vibrational levels, as already indicated above, but also by reactions with ions and neutrals, and the role of these species and corresponding reactions will be discussed below.

3.4.1. Importance of Electron Impact Reactions. The splitting upon electron impact with a CO_2 molecule can in general be considered as a one step process (i.e., reactions 3–8 of Table 5 in the Appendix) or as a two-step process, where the CO_2 molecule is first vibrationally excited, followed by a dissociation reaction of the vibrationally excited molecule.

Figure 4 presents the formation rates of the electron impact reactions with CO_2 in the ground state and with the sum of all

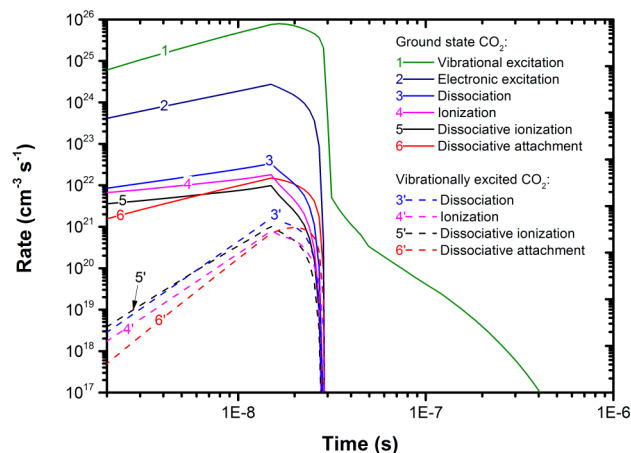


Figure 4. Rates of the different electron impact reactions with ground state CO_2 (solid lines) and vibrationally excited CO_2 (dashed lines) as a function of time during and after one discharge pulse of 30 ns.

vibrationally excited states, for one discharge pulse of 30 ns and its afterglow. The rates of formation for vibrational excitation and electronic excitation from ground state CO_2 molecules are at least 2 orders of magnitude higher than the other reaction rates of formation for the ground state molecules (i.e., dissociation, ionization, dissociative ionization, and attachment). Indeed, as was illustrated in Figure 3, most of the electron energy is transferred to the electronic excited states, and to a lower extent to the vibrational states. However, the threshold energy for vibrational excitation is significant lower (0.083 eV) compared to electronic excitation (7.000 eV), and this explains why the rate of formation for vibrational excitation is still 1 order of magnitude higher than the rate of formation for electronic excitation.⁴³ Moreover, as a result of this low threshold energy, the rate of formation for vibrational excitation decreases much more slowly in the afterglow, where the electron density and temperature are very low (see Figure 2). Indeed, CO_2 can be vibrationally excited even at

atmospheric conditions. The reason is that there are still high energy electrons, capable of electron impact vibrational excitation, present in the tail of the electron energy distribution, even when the electron temperature reaches room temperature.

As mentioned above, Figure 4 also depicts the rates of formation for the electron impact reactions with vibrationally excited CO₂ molecules. It is clear that near the end of the discharge pulse these rates are only about 1 order of magnitude lower than the rates of formation for the corresponding reactions from the ground state. This suggests that the density of the vibrationally excited CO₂ molecules is relatively close to the density of the ground state molecules. Moreover, the activation energy is lower compared to the same reaction with ground state CO₂, as already indicated above by the Fridman–Macheret α -Model.^{10,11} In section 3.4.2, we will discuss in more detail the behavior of vibrationally excited CO₂ molecules, to elucidate whether they really play a role in the splitting process.

3.4.2. Behavior of Vibrationally Excited CO₂ Molecules. In section 3.4.1, it became clear that vibrationally excited CO₂ molecules can be present in rather large amounts, because of the relatively low threshold for vibrational excitation, and as a result, electron impact reactions with vibrationally excited CO₂ molecules occur at a rate of formation which is only 1 order of magnitude lower than the corresponding reactions with ground state CO₂ molecules. However, it is well possible that the vibrationally excited states return to the ground state by relaxation, without resulting in CO₂ splitting. To better understand the formation and the loss of vibrationally excited CO₂ molecules and their role in the plasma, the densities of the various vibrational levels should be compared to the density of ground state CO₂. In Figure 5a the densities of the vibrationally excited levels taken into account in the model, as well as the ground state density of CO₂, are plotted as a function of time, for one discharge pulse of 30 ns and its afterglow. The densities of the vibrationally excited CO₂ molecules are in the order of $1\text{--}8 \times 10^{17} \text{ cm}^{-3}$, which is about 2 orders of magnitude lower than the ground state CO₂ density ($\sim 1.8 \times 10^{19} \text{ cm}^{-3}$). This was already suggested in the previous section, as one of the explanations for the high rates of formation for electron impact reactions with vibrationally excited CO₂. When comparing the different vibrational levels, it is clear that the lowest vibrational state (CO₂v1) has the highest density ($8 \times 10^{17} \text{ cm}^{-3}$ at the maximum), followed by CO₂v2, CO₂v3, and CO₂v4. This can be explained by the lowest threshold for vibrational excitation to the first vibrational state (CO₂v1) and by relaxation of the higher vibrational states to lower levels, controlled by VV transfers (see also below). These transfers cause an increase in the density of the lowest vibrational state after pulse termination, as is clear from Figure 5a, but at $2 \times 10^{-5} \text{ s}$, the density of this lowest vibrational state also starts to decrease. At this point, the density of ground state CO₂ starts to increase again. This suggests that indeed a lot of CO₂ is consumed by vibrational excitation, but eventually most of the vibrationally excited CO₂ molecules relax back to the ground state on a time scale of several 10s or 100s of microseconds. As a DBD consists of many discharge pulses spread in time and volume (see section 3.2), this can eventually cause accumulation effects in the densities of some plasma species, if the interpulse time is shorter than the relaxation time of these species.

To indicate such accumulation effects on the densities of vibrationally excited CO₂ molecules, Figure 5b presents the densities of the different CO₂ vibrational levels and the ground state as a function of time, for five consecutive discharge pulses with a length of 30 ns and an interpulse period of 1 μs . It is clear that the

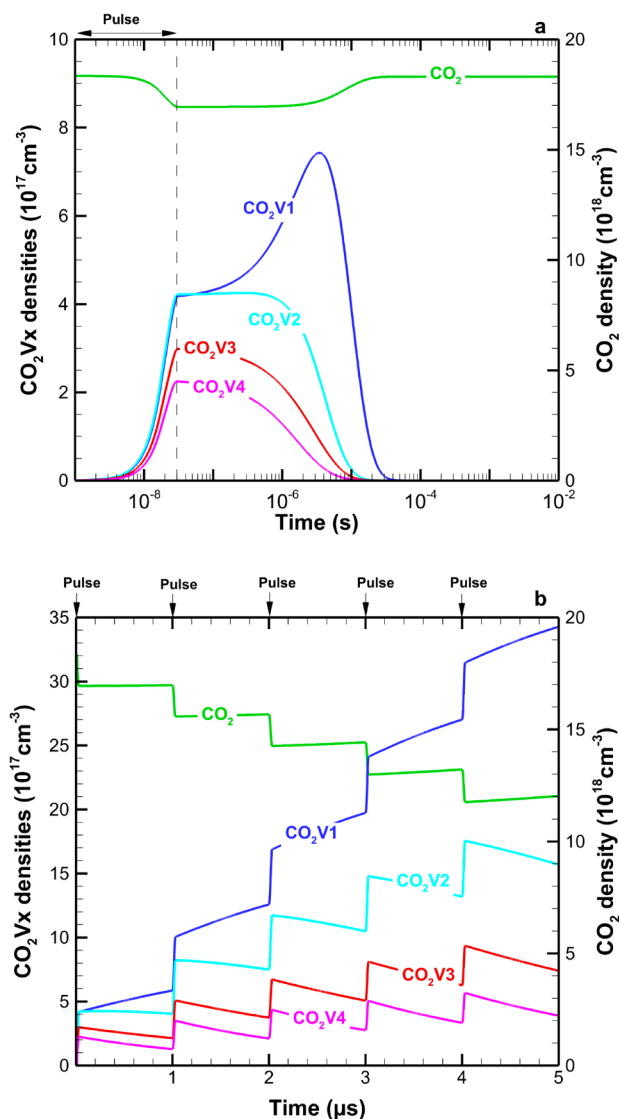


Figure 5. Densities of the vibrationally excited CO₂ species (left y axis) and the ground state CO₂ density (right y axis), as a function of time, during and after one discharge pulse of 30 ns (a), as well as for five consecutive discharge pulses of 30 ns with an interpulse period of 1 μs (b).

higher vibrational levels (i.e., CO₂v4 and CO₂v3) do not exhibit any significant accumulation effects, i.e., their density rises during the pulse, but it drops again in the afterglow to almost the same value when the next pulse starts. The lower vibrational levels, on the other hand, show considerable accumulation, especially CO₂v1. This can again be explained by the VV and VT transfers, leading to relaxation of the higher vibrational levels to the lower levels. The density of the CO₂ ground state molecules drops at each pulse but stays more or less constant in the afterglow or even slightly rises again, which is again attributed to relaxation from the vibrational levels. After five consecutive pulses, the CO₂ ground state density has slightly dropped from 1.7×10^{19} to about $1.2 \times 10^{19} \text{ cm}^{-3}$, whereas the lowest vibrational level of CO₂ has increased nearly 1 order of magnitude, i.e., from 4×10^{17} to $3.5 \times 10^{18} \text{ cm}^{-3}$; hence, it becomes only a factor of 3 lower than the CO₂ ground state density.

It should be stressed, however, that the time between two consecutive pulses (i.e., the interpulse time) is crucial for this accumulation effect. In Figure 6a the net formation of vibrationally excited CO₂ (i.e., the sum of all levels), integrated from the net formation

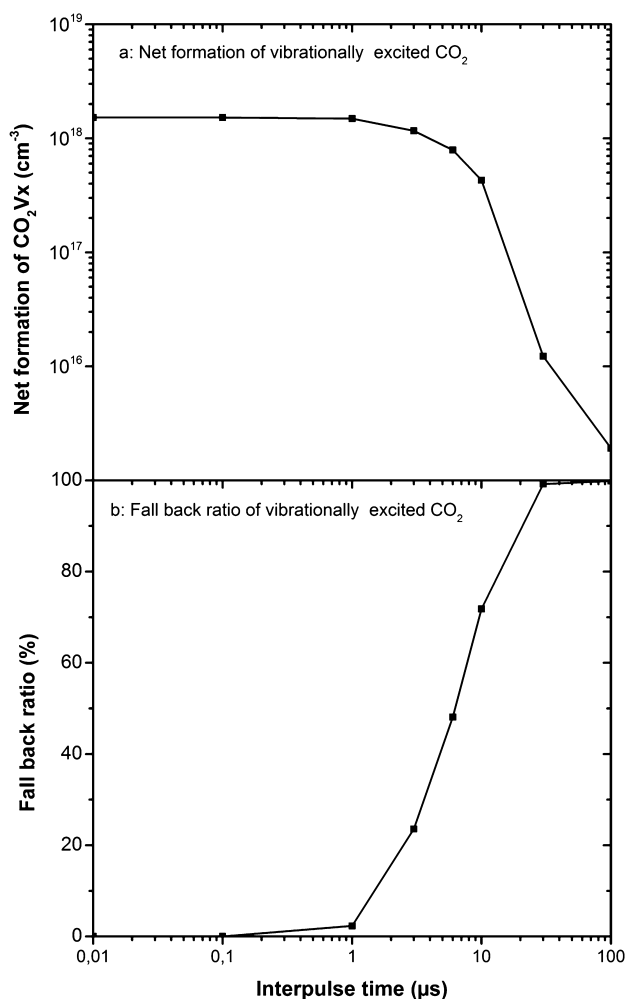


Figure 6. Net formation of vibrationally excited CO₂ (i.e., the sum of all levels) integrated over the time of one (30 ns) pulse and its afterglow (a) and fall back ratio of vibrationally excited CO₂ (i.e., the fraction of vibrational CO₂ that has decayed back to the ground state) (b) for a wide range of interpulse times.

rates over the time of one (30 ns) pulse and its afterglow, is plotted for a wide range of afterglow times or in other words interpulse times, together with the so-called fall back ratio of vibrationally excited CO₂ (i.e., the fraction of vibrational CO₂ that has decayed back to the ground state) in Figure 6b. The figures indicate that, for an interpulse time below 1 μs, a strong accumulation can be expected, as is clear from the high values of the time-integrated net formation and the almost negligible fall back ratio. This was also obvious from Figure 5b. For an interpulse time between 1 and 10 μs, however, a fraction ranging from 2 to 72% of the vibrationally excited CO₂ falls back to the ground state, and as a result the time-integrated net formation drops by a factor of ±2. This means that the accumulation effect on the vibrationally excited states becomes less important. If the interpulse time exceeds 10 μs, most of the vibrationally excited CO₂ molecules will decay back to the ground state before the next pulse starts, and the net formation drops by roughly 3 orders of magnitude. Hence, the accumulation effects for the vibrationally excited levels become negligible.

It should be realized that we do not exactly know the interpulse time between two filaments in a DBD, but it is likely that some molecules pass a couple of microdischarges locally in a time frame of 1 μs. If this is true, then this accumulation effect, and the

role of vibrational levels, might be important, even in a DBD. More in general, it would be very interesting to utilize this accumulation effect to increase the efficiency of CO₂ splitting, by means of a pulsed power deposition system.

3.4.3. Behavior of Neutrals in the Plasma. If we want to identify the dominant splitting pathways for CO₂, not only the electrons and the vibrational species should be investigated but also the neutral species and the ions. In Figure 7a,b the densities

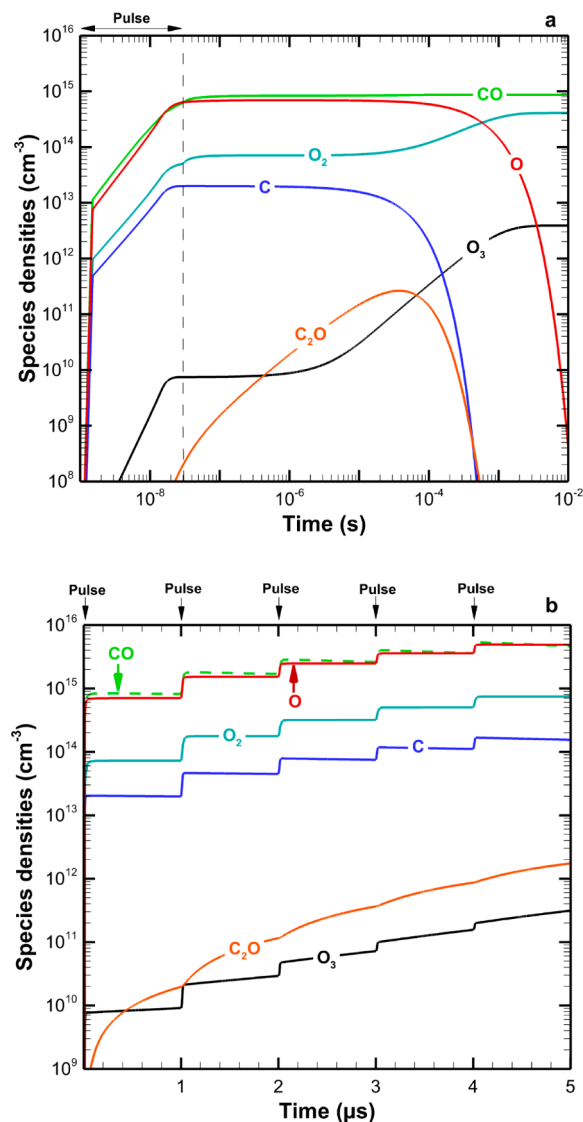
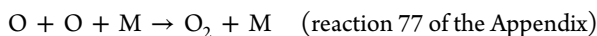


Figure 7. Densities of the important neutral species as a function of time, during and after one discharge pulse of 30 ns (a) as well as for five consecutive discharge pulses of 30 ns with an interpulse period of 1 μs (b).

of the most important neutral species formed in the CO₂ plasma are plotted as a function of time, for one pulse of 30 ns and its afterglow (a) as well as for five consecutive pulses with an interpulse period of 1 μs (b). Figure 7a indicates CO, molecular oxygen, and ozone are the main reaction products at the long time scale, although ozone is produced with a density of at least 2 orders of magnitude lower than CO and oxygen. This explains why in the literature CO and O₂ were only identified as reaction products.^{3,7,44} Atomic oxygen reaches densities similar to CO ($\sim 1 \times 10^{15}$ cm⁻³) during the pulse and in the afterglow until about 100 μs, but then it starts to drop very fast to negligible

values, which causes the densities of molecular oxygen and ozone to increase. This increase is a consequence of the following third body reactions



These reactions have maximum rates of formation of 10^{17} and $10^{15} \text{ cm}^{-3} \text{ s}^{-1}$, respectively, at around 30 ns.

Figure 7a also indicates other carbon containing species (i.e., C and C_2O) as reaction byproducts with relatively high densities. As these species have the ability to oxidize in the presence of strong oxidizers (i.e., atomic and molecular oxygen) they eventually favor the production of CO, as well as CO_2 again (reactions 70–73 of the Appendix), with a maximum rate of formation at around $10^{16} \text{ cm}^{-3} \text{ s}^{-1}$, at 10 μs .

Similar as in the previous section, the effect of accumulating neutral species is illustrated by simulating five consecutive pulses of 30 ns, with an interpulse period of 1 μs , as presented in Figure 7b. The neutral species indeed accumulate, as a result of their longer lifetime compared to excited species, i.e. for the conditions under study the lifetime was typically calculated to be lower than a few μs for the vibrationally excited CO_2 molecules (cf. Figure 6b above) vs $>1 \mu\text{s}$ for the neutral species. The species with the highest densities accumulate stepwise by every nanosecond pulse, followed by a steady state or a small decrease in density during the afterglow. A more significant effect can be observed for C_2O and O_3 , which are characterized by a more or less continuous increase, not only during the pulse but also during the afterglow. However, the density of C_2O will drop dramatically at longer time scales, as was illustrated in Figure 7a for one pulse. This is not the case for ozone, which is quite stable at mild conditions (400 K), with a dissociation rate coefficient of $1.603 \times 10^{-22} \text{ cm}^3 \text{ s}^{-1}$ (reaction 75 of the Appendix). As a consequence, the ozone density will always increase by accumulation even at longer interpulse periods above 1 μs .

3.4.4. Behavior of Ions in the Plasma. As illustrated in section 3.4.1, a significant fraction of the electron energy is transferred to ionization at typical E/n values characteristic for a DBD. Therefore, Figure 8a presents the densities of the most important ions as a function of time, for the 30 ns pulse and its afterglow. Most small ions (i.e., C^+ , O^+ , O^- , and O_2^+) recombine immediately after pulse termination, and hence their densities drop significantly to negligible values. The larger ions, such as CO_2^+ , CO^+ , C_2O_2^+ , C_2O_3^+ , and C_2O_4^+ , recombine later at around 1 microsecond. Finally, some long living ions (i.e., CO_4^- , CO_4^+ , and CO_3^-) are identified in our model that recombine very slowly even after 1 ms. It should be mentioned, however, that although the ion chemistry used in this model is quite large, it is well possible that for these long living ions some loss mechanisms are not taken into account, as these ions are not so common and maybe not all their processes are known in literature. So it might be that the long lifetimes of these ions are somewhat overestimated. Nevertheless, this is not so important for the present study, as we will demonstrate below that the ions do not play a significant role in the CO_2 splitting mechanism.

Again, the densities of some ions can increase due to accumulation in consecutive pulses, as shown in Figure 8b, where the densities of the long-living ions are depicted for five consecutive pulses of 30 ns with an interpulse period of 1 μs . Note that the densities of the short-living ions are not plotted, as they exhibit a peak during the pulse, but negligible values in between two pulses, as is clear from Figure 8a. Except for the CO_4^- ions,

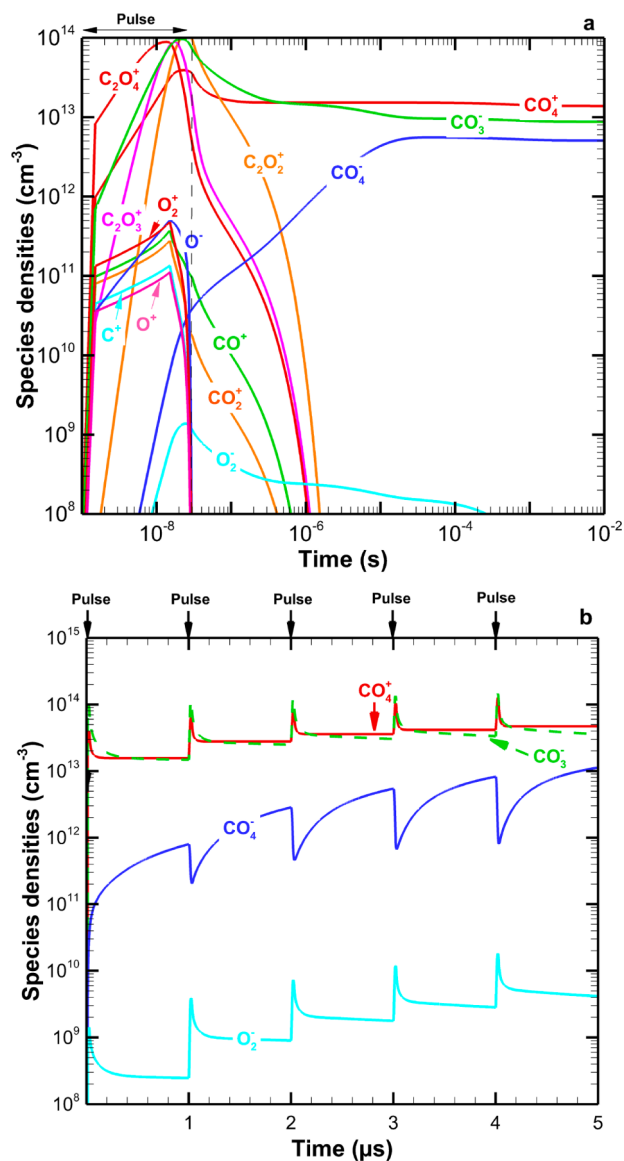


Figure 8. Densities of the ions as a function of time, during and after one discharge pulse of 30 ns (a) as well as for five consecutive discharge pulses of 30 ns with an interpulse period of 1 μs (b). Note that in (b) only those ions are shown that do not disappear immediately after pulse termination. The other ions are only characterized by a peak at each pulse, as can be derived from (a).

the density of the other long-living ions typically increases for each pulse, followed by a recombination period where the density decreases. No significant accumulation effect is observed for CO_4^+ and CO_3^- , and as a result, their density stays more or less constant in a pulsed power deposition system. The O_2^- density shows a somewhat different behavior: it increases with 1 order of magnitude during the pulse, and it drops by only half an order of magnitude in between two pulses, so that accumulation effects are apparent. However, their maximum density is still very low compared to the other ions illustrated in Figure 8b. Finally, the CO_4^- density is characterized by the opposite behavior: it decreases during each pulse (except for the first pulse) and increases during the interpulse period. This can be explained as follows. CO_4^- is mainly produced by the third body reaction between O_2^- and CO_2 (reaction 84 of the Appendix) and consumed by recombination with CO_2^+ and C_2O_2^+ (reactions 104

and 111) to form CO_2 , CO , and O_2 . Hence, CO_4^- recombines during every pulse with these positive ions, until the pulse stops (and CO_2^+ and C_2O_2^+ decrease in density), and subsequently CO_4^- is only produced, from O_2^- , which recombines more slowly than CO_2^+ and C_2O_2^+ .

3.4.5. Contribution of the Various Plasma Species to the CO_2 Splitting. Up to this point we only presented the densities of the vibrationally excited CO_2 molecules, the other neutral species and the ions separately from the splitting of CO_2 , but this does not yet give an answer to the question “which species and reactions contribute most to the CO_2 splitting?” Therefore, in Figure 9a,b the rates of the reactions, involving ions and neutral

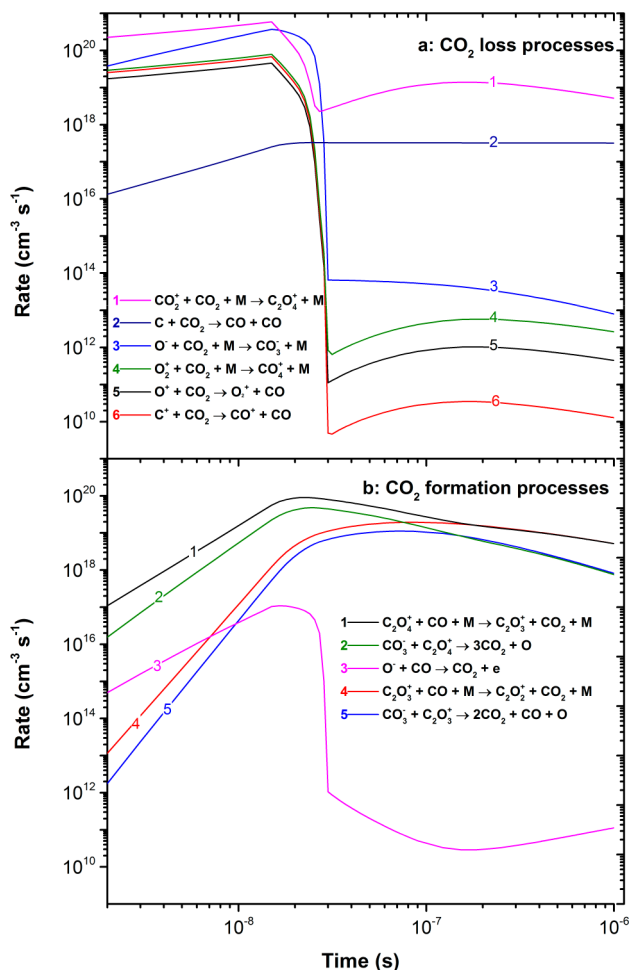


Figure 9. Rates for CO_2 loss (a) and formation (b) by the most important ion and neutral reactions, as a function of time during and after one discharge pulse of 30 ns.

species, contributing to the loss and production of CO_2 , respectively, are plotted as a function of time during a 30 ns pulse and its afterglow. If we compare these rates with the rates of formation of the electron impact reactions with CO_2 (Figure 4), it is clear that the electron impact vibrational and electronic excitation rates of formation are 6 and 4 orders of magnitude higher than the rates of the highest ion-induced loss reactions of CO_2 , and the electron impact dissociation, ionization, dissociative ionization and attachment production rates are about 2 orders of magnitude higher. However, as already mentioned in section 3.4.2, electron impact vibrational and electronic excitation do not necessarily lead to the splitting of CO_2 , because a considerable

fraction of the excited states can relax back to the ground state of CO_2 . The same applies to ionization, because the CO_2^+ ions mostly recombine upon pulse termination, forming again CO_2 molecules. However, electron impact dissociation and dissociative ionization and attachment definitely give rise to splitting of the CO_2 molecules, and the rates of these reactions are also higher than the highest ion or neutral induced reactions, as is obvious from comparing Figure 4 with Figure 9a. This tells us that electron impact reactions are mainly responsible for the CO_2 splitting, and that the contribution of ion and neutral reactions can be neglected, at least during the pulse.

Looking at the afterglow, the rates of formation for the electron induced reactions drop significantly upon pulse termination, as illustrated in Figure 4 above, but the same applies to the rates of most reactions involving ions, which also decrease over several orders of magnitude as a result of recombination processes (see curves 1, 3–6 in Figure 9a). This is not the case for the three-body reaction with CO_2^+ ions (curve 1 in Figure 9a), for which the CO_2 loss rate drops by 2 orders of magnitude at the end of the pulse, but remains more or less constant in the early afterglow, within a time frame of 1 microsecond. However, after 1 microsecond, the CO_2 loss rate decreases very quickly (not shown, because out of scale), corresponding to the density profile of CO_2^+ in Figure 8a. The neutrals do not contribute much to the loss of CO_2 , except for the reaction between C and CO_2 producing two CO molecules (curve 2 in Figure 9a, and reaction 65 from the Appendix). Looking at the C atom density in Figure 7a, the CO_2 loss rate of this reaction is expected to remain constant in a time frame up to 0.1 ms, followed by a fast decay afterward.

To identify the actual net contribution of the various species to the loss of CO_2 , the significant production reactions of CO_2 should also be accounted for. Their rates of formation are also plotted as a function of time during the 30 ns pulse and its afterglow in Figure 9b. It is clear that most of the CO_2 production can be allocated to the same ions (namely C_2O_4^+ and CO_3^+) produced in the CO_2 loss processes by ions, except for C_2O_3^+ and O^- . Moreover, the sum of the rates for CO_2 formation and loss by ions have more or less the same magnitude and therefore the net contribution of ions to the CO_2 splitting will not be significant compared to the net contribution of the electron impact reactions. The formation of CO_2 by neutrals, on the other hand, is close to zero, meaning that their net contribution to the CO_2 splitting is determined only by their CO_2 loss rates. However, as illustrated in Figure 9a, this CO_2 loss rate is very low compared to the CO_2 loss rates of the ion reactions and certainly to the CO_2 loss rates of the electron impact reactions, so their contribution will also be negligible.

To further quantify the role of the various species and reactions to the CO_2 splitting, the time integrated contributions of the various processes are presented in Table 3, for the 30 ns pulse, an afterglow of 0.1 s, and their sum. It is clear that most of the CO_2 molecules are lost by vibrational excitation (cf. the high values of their time-integrated rates, presented in Table 3). However, keeping in mind that most of these excited species might return to the ground state when the afterglow is long enough (see section 3.4.2 above), we will focus on the electron impact reactions which cause a direct dissociation (or ionization, or dissociative ionization or attachment) of CO_2 . As can be seen in Table 3, the pulse period has obviously the highest contribution to the loss of CO_2 , in spite of its short time-scale, and this is almost exclusively due to the electron impact reactions (i.e., dissociation, ionization, dissociative ionization and attachment). Indeed, the contribution of the neutral reactions is several orders

Table 3. Overview of the Time-Integrated Net Rates of the Different Reaction Types Contributing to the Loss of Ground State CO₂, during a Pulse of 30 ns, an Afterglow of 0.1 s, and the Sum of Both, As Well As the Net Overall Contributions (in %) for the Actual Dissociation of the CO₂ Ground State Molecules^a

reactions	pulse (cm ⁻³)	afterglow (cm ⁻³)	pulse + afterglow (cm ⁻³)	overall contribution to CO ₂ splitting (%)
electron impact vibrational excitation	1.5 × 10 ¹⁸	3.8 × 10 ¹⁴	1.5 × 10 ¹⁸	
electron impact electronic excitation	3.9 × 10 ¹⁶		3.9 × 10 ¹⁶	
electron impact dissociation	4.8 × 10 ¹⁴		4.8 × 10 ¹⁴	(52%)
electron impact ionization	2.6 × 10 ¹⁴		2.6 × 10 ¹⁴	(29%)
electron impact dissociative ionization	1.4 × 10 ¹⁴		1.4 × 10 ¹⁴	(16%)
electron impact dissociative attachment	2.2 × 10 ¹⁴		2.2 × 10 ¹⁴	(23%)
ion reactions	-1.2 × 10 ¹⁴	-8.5 × 10 ¹³	-2.0 × 10 ¹⁴	(-22%)
neutral reactions	7.4 × 10 ⁹	1.9 × 10 ¹³	1.9 × 10 ¹³	(2%)

^aThe time-integrated vibrational and electronic excitation rates are also listed, to illustrate the dominant role of these processes in the plasma, but they do not (directly) contribute to the CO₂ splitting and are therefore not included in the calculation of the overall contributions presented in the last column.

of magnitude lower, and the ion induced reactions cause even a net formation of CO₂, as also reported by Indarto et al.⁸ In the afterglow, the electron impact reactions do not contribute to the CO₂ splitting, because of too low values for the electron density and temperature. In contrast, the contribution of the neutrals increases by almost 4 orders of magnitude (~10⁹ vs ~10¹³ cm⁻³), which is mainly attributed to the long time-scale of the afterglow assumed here. Nevertheless, this contribution is still significantly lower than the electron contributions during the pulse. Again, the ions contribute only to the net formation of CO₂ in the afterglow.

The overall (i.e., sum of pulse and afterglow) net contribution to the loss of CO₂ can be completely assigned to electron impact reactions, especially to electron impact dissociation (with a contribution of 52%). Electron impact ionization and dissociative ionization also contribute for 29% and 16%, respectively, but this is partly compensated by the “negative contribution” (-22%) of the ion reactions. Indeed, the ions formed by electron impact (dissociative) ionization, or by further charge exchange reactions of the formed ions, will mostly recombine again, i.e., they contribute only to the formation of CO₂, so that the net contribution of ionization (including dissociative ionization) should be interpreted as around 23%. The same value of 23% was also found to be the contribution of dissociative attachment. Finally, the neutrals contribute only by 2%, in case of such a long afterglow (0.1 s), but if the afterglow will be shorter, as is well possible in a filamentary DBD, the contribution of neutrals to the CO₂ splitting will become negligible. In fact, the contribution of the neutrals can be fully allocated to one reaction, i.e., C + CO₂ → 2 CO (see Figure 9).

As we want to elucidate the role of vibrationally excited CO₂ molecules, the same calculation as for Table 3 was carried out to obtain Table 4, which represents the different reactions taking place with the sum of all vibrationally excited CO₂ molecules, and their corresponding time integrated contributions during the pulse, the afterglow, and the sum of both. The first line of Table 4 indicates the time-integrated relaxation rate by VV and VT transfers to the CO₂ ground state. It is clear that the overall integrated rate of these relaxation processes (i.e., during pulse + afterglow) is exactly the same as the integrated rate of vibrational excitation of CO₂ (i.e., 1.5 × 10¹⁸ cm⁻³), meaning that all vibrationally excited CO₂ molecules return back to the ground state without contributing to the CO₂ splitting, at least when assuming such a long afterglow. It is, however, important to stress that if the afterglow is shorter, this is not the case, as was elaborated in section 3.4.2 above. In any case, these relaxation processes obviously do not contribute to the CO₂ splitting, and are therefore

Table 4. Overview of the Time-Integrated Net Rates of the Different Reaction Types Contributing to the Loss of Vibrationally Excited CO₂, during a Pulse of 30 ns, an Afterglow of 0.1s, and the Sum of Both, As Well As the Net Overall Contributions (in %) for the Actual Dissociation of the Vibrationally Excited CO₂ Molecules^a

reactions	pulse (cm ⁻³)	afterglow (cm ⁻³)	pulse + afterglow (cm ⁻³)	overall contribution to CO ₂ splitting (%)
relaxation	1.1 × 10 ¹⁵	1.5 × 10 ¹⁸	1.5 × 10 ¹⁸	
electron impact dissociation	1.2 × 10 ¹³		1.2 × 10 ¹³	(19%)
electron impact ionization	5.1 × 10 ¹²		5.1 × 10 ¹²	(8%)
electron impact dissociative ionization	2.2 × 10 ¹²		2.2 × 10 ¹²	(4%)
electron impact dissociative attachment	7.0 × 10 ¹²		7.0 × 10 ¹²	(11%)
ion reactions	3.0 × 10 ¹³	6.7 × 10 ¹²	3.6 × 10 ¹³	(57%)
neutral reactions	2.1 × 10 ⁹	8.4 × 10 ¹¹	8.4 × 10 ¹¹	(1%)

^aThe time-integrated (VV and VT) relaxation rate is also listed, to illustrate the importance of this process, but it does obviously not contribute to the CO₂ splitting and is therefore not included in the calculation of the overall contributions presented in the last column.

not included in our calculation of the relative contributions in the last column of Table 4.

Looking closer to the processes which can cause dissociation of the vibrationally excited CO₂ molecules during the pulse, the electron impact reaction rates are at least 1 order of magnitude lower than the same reactions with ground state CO₂. Indeed the rate coefficients of the reactions with vibrationally excited CO₂ molecules are larger compared to the same reactions with ground state CO₂, but their densities are at least 2 orders of magnitude lower (see section 3.4.1 above). As far as the ion reactions are concerned, in contrast with ground state CO₂, the ion reactions with vibrationally excited CO₂ contribute quite significantly to the net loss, with an overall contribution of 57%, followed by electron impact dissociation (19%) and dissociative attachment (11%). Ionization and dissociative ionization of vibrationally excited CO₂ contribute for only 8 and 4%, respectively, which is lower than their contribution for ground state CO₂. This can be explained by their high threshold energy (i.e., 13.3 eV), which is still clearly higher than the energy of the vibrational levels (i.e., ~1 eV), so that the advantage of a lower threshold for

Table 5. Overview of the Electron Impact Reactions Included in the Model, As Well As the References from Where the Cross Sections Were Adopted^a

no.	reaction	reaction type	rate coefficient	ref
(1)	$e^- + \text{CO}_2 \rightarrow \text{ev} + \text{CO}_2$	momentum transfer	$f(\sigma)$	25
(2)	$e^- + \text{CO}_2 \rightarrow e^- + e^- + \text{CO}_2^+$	ionization	$f(\sigma)$	25,26
(3)	$e^- + \text{CO}_2 \rightarrow e^- + e^- + \text{CO}^+ + \text{O}$	dissociative ionization	$f(\sigma)$	25,26
(4)	$e^- + \text{CO}_2 \rightarrow e^- + e^- + \text{C}^+ + \text{O}_2$	dissociative ionization	$f(\sigma)$	25,26
(5)	$e^- + \text{CO}_2 \rightarrow e^- + e^- + \text{O}^+ + \text{CO}$	dissociative ionization	$f(\sigma)$	25,26
(6)	$e^- + \text{CO}_2 \rightarrow e^- + e^- + \text{O}_2^+ + \text{C}$	dissociative ionization	$f(\sigma)$	25,26
(7)	$e^- + \text{CO}_2 \rightarrow \text{O}^- + \text{CO}$	electron attachment	$f(\sigma)$	25
(8)	$e^- + \text{CO}_2 \rightarrow e^- + \text{CO} + \text{O}$	dissociation	$f(\sigma)$	25
(9)	$e^- + \text{CO}_2 \rightarrow e^- + \text{CO}_2\text{v1}$	vibrational excitation	$f(\sigma)$	25
(10)	$e^- + \text{CO}_2 \rightarrow e^- + \text{CO}_2\text{v2}$	vibrational excitation	$f(\sigma)$	25
(11)	$e^- + \text{CO}_2 \rightarrow e^- + \text{CO}_2\text{v3}$	vibrational excitation	$f(\sigma)$	25
(12)	$e^- + \text{CO}_2 \rightarrow e^- + \text{CO}_2\text{v4}$	vibrational excitation	$f(\sigma)$	25
(13)	$e^- + \text{CO}_2 \rightarrow e^- + \text{CO}_2\text{e1}$	electronic excitation	$f(\sigma)$	25
(14)	$e^- + \text{CO}_2 \rightarrow e^- + \text{CO}_2\text{e2}$	electronic excitation	$f(\sigma)$	25
(15)	$e^- + \text{CO} \rightarrow e^- + \text{CO}$	momentum transfer	$f(\sigma)$	27
(16)	$e^- + \text{CO} \rightarrow e^- + e^- + \text{CO}^+$	ionization	$f(\sigma)$	28
(17)	$e^- + \text{CO} \rightarrow e^- + e^- + \text{C}^+ + \text{O}$	dissociative ionization	$f(\sigma)$	28
(18)	$e^- + \text{CO} \rightarrow e^- + e^- + \text{C} + \text{O}^+$	dissociative ionization	$f(\sigma)$	28
(19)	$e^- + \text{CO} \rightarrow \text{O}^- + \text{C}$	electron attachment	$f(\sigma)$	28
(20)	$e^- + \text{CO} \rightarrow e^- + \text{C} + \text{O}$	dissociation	$f(\sigma)$	28
(21)	$e^- + \text{CO} \rightarrow e^- + \text{COv1}$	vibrational excitation	$f(\sigma)$	28
(22)	$e^- + \text{CO} \rightarrow e^- + \text{COe1}$	electronic excitation	$f(\sigma)$	28
(23)	$e^- + \text{CO} \rightarrow e^- + \text{COe2}$	electronic excitation	$f(\sigma)$	28
(24)	$e^- + \text{CO} \rightarrow e^- + \text{COe3}$	electronic excitation	$f(\sigma)$	28
(25)	$e^- + \text{CO} \rightarrow e^- + \text{COe4}$	electronic excitation	$f(\sigma)$	28
(26)	$e^- + \text{C} \rightarrow e^- + \text{C}$	momentum transfer	$f(\sigma)$	45
(27)	$e^- + \text{C} \rightarrow e^- + e^- + \text{C}^+$	dissociative ionization	$f(\sigma)$	45
(28)	$e^- + \text{C}_2 \rightarrow e^- + \text{C}_2$	momentum transfer	$f(\sigma)$	46
(29)	$e^- + \text{C}_2 \rightarrow e^- + \text{C} + \text{C}$	dissociation	$f(\sigma)$	46
(30)	$e^- + \text{C}_2 \rightarrow e^- + e^- + \text{C}_2^+$	ionization	$f(\sigma)$	46
(31)	$e^- + \text{O}_2 \rightarrow e^- + \text{O}_2$	momentum transfer	$f(\sigma)$	29
(32)	$e^- + \text{O}_2 \rightarrow e^- + \text{O} + \text{O}$	dissociation	$f(\sigma)$	29
(33)	$e^- + \text{O}_2 \rightarrow e^- + e^- + \text{O}_2^+$	ionization	$f(\sigma)$	29
(34)	$e^- + \text{O}_2 \rightarrow e^- + e^- + \text{O} + \text{O}^+$	dissociative ionization	$f(\sigma)$	47
(35)	$e^- + \text{O}_2 \rightarrow \text{O}^- + \text{O}$	dissociation	$f(\sigma)$	29
(36)	$e^- + \text{O}_2 \rightarrow e^- + \text{O}_2\text{v1}$	vibrational excitation	$f(\sigma)$	29
(37)	$e^- + \text{O}_2 \rightarrow e^- + \text{O}_2\text{v2}$	vibrational excitation	$f(\sigma)$	29
(38)	$e^- + \text{O}_2 \rightarrow e^- + \text{O}_2\text{v3}$	vibrational excitation	$f(\sigma)$	29
(39)	$e^- + \text{O}_2 \rightarrow e^- + \text{O}_2\text{e1}$	electronic excitation	$f(\sigma)$	29
(40)	$e^- + \text{O}_2 \rightarrow e^- + \text{O}_2\text{e2}$	electronic excitation	$f(\sigma)$	29
(41)	$e^- + \text{O}_3 \rightarrow e^- + \text{O}_3$	momentum transfer	$f(\sigma)$	48
(42)	$e^- + \text{O}_3 \rightarrow e^- + \text{O}_2 + \text{O}$	dissociation	$f(\sigma)$	49
(43)	$e^- + \text{O}_3 \rightarrow e^- + e^- + \text{O}_2^+ + \text{O}$	Dissociative ionization	$f(\sigma)$	49
(44)	$e^- + \text{O}_3 \rightarrow e^- + \text{O}^+ + \text{O}^- + \text{O}$	dissociative ionization	$f(\sigma)$	49
(45)	$e^- + \text{O}_3 \rightarrow \text{O}^- + \text{O}_2$	electron attachment	$f(\sigma)$	50
(46)	$e^- + \text{O}_3 \rightarrow \text{O} + \text{O}_2^-$	electron attachment	$f(\sigma)$	50

Table 5. continued

no.	reaction	reaction type	rate coefficient	ref
(47)	$e^- + O \rightarrow e^- + O$	momentum transfer	$f(\sigma)$	51
(48)	$e^- + O \rightarrow e^- + e^- + O^+$	ionization	$f(\sigma)$	52

^aNote: The electron impact dissociation reaction of CO₂ (i.e., reaction 8) proceeds through electron impact excitation, followed by dissociation. The electron impact electronic excitation reactions of CO₂ (i.e., reactions 13 and 14), on the other hand, form excited levels which decay back to the ground state, without dissociation. The same is true for the electron impact dissociation and electronic excitations of CO (reaction 20 and reactions 22–25, respectively) and O₂ (reaction 32 and reactions 39–40, respectively).

Table 6. Overview of the Electron-Ion Recombinations and Electron Attachment Reactions Included in the Model, As Well As the Corresponding Rate Coefficients and References from Where These Data Were Adopted

no.	reaction	rate coefficient	ref
(49)	$e^- + CO_2^+ \rightarrow CO + O$	$2 \times 10^{-5} \times Tg^{1-} \times Te(eV)^{-0.5}$ $cm^3 s^{-1}$	53
(50)	$e^- + CO_2^+ \rightarrow C + O_2$	$3.939 \times 10^{-7} \times Te(eV)^{-0.4} cm^3 s^{-1}$	26
(51)	$e^- + CO_4^+ \rightarrow CO_2 + O_2$	$1.608 \times 10^{-7} \times Te(eV)^{-0.5} cm^3 s^{-1}$	26
(52)	$e^- + CO^+ \rightarrow C + O$	$3.683 \times 10^{-8} \times Te(eV)^{-0.55} cm^3 s^{-1}$	28
(53)	$e^- + C_2O_2^+ \rightarrow CO + CO$	$4.0 \times 10^{-7} \times Te(eV)^{-0.34} cm^3 s^{-1}$	54
(54)	$e^- + C_2O_3^+ \rightarrow CO_2 + CO$	$5.4 \times 10^{-8} \times Te(eV)^{-0.7} cm^3 s^{-1}$	54
(55)	$e^- + C_2O_4^+ \rightarrow CO_2 + CO_2$	$2.0 \times 10^{-5} \times Tg^{1-} \times Te^{-0.5} cm^3 s^{-1}$	54
(56)	$e^- + C_2^+ \rightarrow C + C$	$1.79 \times 10^{-8} \times Te(eV)^{-0.5} cm^3 s^{-1}$	54
(57)	$e^- + O_2 + M \rightarrow O_2^- + M$	$3 \times 10^{-30} cm^6 s^{-1}$	35
(58)	$e^- + O_3 + M \rightarrow O_3^- + M$	$5 \times 10^{-31} \times Te(eV)^{-0.5} cm^6 s^{-1}$	54
(59)	$e^- + O + M \rightarrow O^- + M$	$10^{-31} cm^6 s^{-1}$	35
(60)	$e^- + O_2^+ + M \rightarrow O_2 + M$	$10^{-26} cm^6 s^{-1}$	55
(61)	$e^- + O_2^+ \rightarrow O + O$	$6 \times 10^{-7} \times Tg(K)^{-0.5} \times Te(eV)^{-0.5}$ $cm^3 s^{-1}$	53
(62)	$e^- + O^+ + M \rightarrow O + M$	$10^{-26} cm^6 s^{-1}$	55
(63)	$e^- + O_4^+ \rightarrow O_2 + O_2$	$2.251 \times 10^{-7} \times Te(eV)^{-0.5} cm^3 s^{-1}$	34

ionization from the vibrational levels is limited. Indeed, the electronically excited states are more suitable for stimulating ionization than the vibrationally excited states (see section 2.2).

Finally, to distinguish between the actual contribution of the vibrationally excited levels and of the ground state to the CO₂ splitting, we need to compare the sum of the net contributions of ground state CO₂ with the sum of the net contributions of vibrationally excited CO₂, both integrated during the pulse and the afterglow. Integrated over pulse and afterglow, the total loss of CO₂ from ground state molecules amounts to $9.2 \times 10^{14} cm^{-3}$, whereas the total loss of CO₂ from the vibrational levels is $6.3 \times 10^{13} cm^{-3}$. This means that the majority (i.e., 94%) of the CO₂ splitting occurs by reactions with ground state CO₂ and only 6% by reactions with vibrationally excited CO₂. It should be realized, however, that these estimations are performed for one pulse and a long afterglow, and that the actual contribution of vibrationally excited CO₂ could be (much) higher in a DBD, attributed to accumulation effects due to consecutive pulses, depending on the interpulse period between successive filaments, as discussed in detail in section 3.4.2 above.

Eventually the influence of vibrationally excited CO₂ molecules can be summarized as follows:

1. Vibrationally excited CO₂ molecules have a high density compared to the other CO₂ splitting species in the plasma.

Table 7. Overview of the Neutral Reactions Included in the Model, As Well As the Corresponding Rate Coefficients and References from Where These Data Were Adopted

no.	reaction	rate coefficient	ref
(64)	$O + CO_2 \rightarrow CO + O_2$	$2.8 \times 10^{-11} \times \exp(-26500/Tg(K)) cm^3 s^{-1}$	26
(65)	$C + CO_2 \rightarrow CO + CO_2$	$1.0 \times 10^{-15} cm^3 s^{-1}$	54
(66)	$O + CO_2 + M \rightarrow CO_2 + M$	$8.2 \times 10^{-34} \times \exp(-1510/Tg(K))$	35
(67)	$O_2 + CO \rightarrow CO_2 + O$	$4.2 \times 10^{-12} \times \exp[-24000/Tg(K)] cm^3 s^{-1}$	26
(68)	$O_3 + CO \rightarrow CO_2 + O_2$	$4.0 \times 10^{-25} cm^3 s^{-1}$	26
(69)	$C + CO + M \rightarrow C_2O + M$	6.5×10^{-32}	35
(70)	$O_2 + C \rightarrow CO + O$	$3.0 \times 10^{-11} cm^3 s^{-1}$	35
(71)	$O + C + M \rightarrow CO + M$	$2.136 \times 10^{-29} \times (Tg(K)/300)^{-3.08} \times \exp(2114/Tg(K)) cm^6 s^{-1}$	26
(72)	$O + C_2O \rightarrow CO + CO$	$5.0 \times 10^{-11} cm^3 s^{-1}$	54
(73)	$O_2 + C_2O \rightarrow CO_2 + CO$	$3.3 \times 10^{-13} cm^3 s^{-1}$	35
(74)	$O + O_3 \rightarrow O_2 + O_2$	$3.1e-14 \times Tg(K)^{0.75} \times \exp[-1575/Tg(K)] cm^3 s^{-1}$	35
(75)	$O_3 + M \rightarrow O_2 + O + M$	$4.1175 \times 10^{-10} \times \exp(-11430/Tg(K)) cm^3 s^{-1}$	26
(76)	$O + O_2 + M \rightarrow O_3 + M$	$1.81 \times 10^{-33} \times (Tg(K)/300)^{-1.2}$	35
(77)	$O + O + M \rightarrow O_2 + M$	$1.27 \times 10^{-32} \times (Tg(K)/300)^{-1} \times \exp(-170/Tg(K)) cm^6 s^{-1}$	56

2. The influence of accumulation can play a role for the lower vibrational states and must be considered in DBDs, which consist of successive pulses (filaments).
3. The activation energy of the reactions with vibrationally excited CO₂ is lower compared to the same reactions with ground state CO₂.
4. The vibrationally excited CO₂ molecules will, however, eventually relax back to the ground state, if the afterglow (i.e., interpulse period) is long enough, so that their net contribution to the CO₂ splitting is estimated to be limited to 6%.
5. This contribution can, however, be much larger if the interpulse period between successive filaments is shorter, so that accumulation effects become important.

4. CONCLUSIONS

We have investigated the plasma chemistry in a DBD operating in pure CO₂, including the role of vibrationally excited levels, and we were able to identify the important species and reactions playing a role in the CO₂ splitting. We should, however, point out that the vibrational excitation of CO and O₂ could also play an important role in the plasma, especially in long time scale simulations where the CO and O₂ densities will build up. The effect of these vibrational levels is not yet taken into account in our present

Table 8. Overview of Ion-Neutral and Ion-Ion Reactions Included in the Model, As Well As the Corresponding Rate Coefficients and References from Where These Data Were Adopted

no.	reaction	rate coefficient	ref
(78)	$O_2^+ + CO_2 + M \rightarrow CO_4^+ + M$	$2.3 \times 10^{-29} \text{ cm}^6 \text{ s}^{-1}$	26
(79)	$O^+ + CO_2 \rightarrow O_2^+ + CO$	$9.4 \times 10^{-10} \text{ cm}^3 \text{ s}^{-1}$	26
(80)	$O^+ + CO_2 \rightarrow CO_2^+ + O$	$4.5 \times 10^{-10} \text{ cm}^3 \text{ s}^{-1}$	26
(81)	$C^+ + CO_2 \rightarrow CO^+ + CO$	$1.1 \times 10^{-9} \text{ cm}^3 \text{ s}^{-1}$	57
(82)	$CO^+ + CO_2 \rightarrow CO_2^+ + CO$	$1.0 \times 10^{-9} \text{ cm}^3 \text{ s}^{-1}$	57
(83)	$O^- + CO_2 + M \rightarrow CO_3^- + M$	$9.0 \times 10^{-29} \text{ cm}^6 \text{ s}^{-1}$	53
(84)	$O_2^- + CO_2 + M \rightarrow CO_4^- + M$	$1.0 \times 10^{-29} \text{ cm}^6 \text{ s}^{-1}$	53
(85)	$O_3^- + CO_2 \rightarrow O_2 + CO_3^-$	$5.5 \times 10^{-10} \text{ cm}^3 \text{ s}^{-1}$	35
(86)	$O_4^- + CO_2 \rightarrow CO_4^- + O_2$	$4.8 \times 10^{-10} \text{ cm}^3 \text{ s}^{-1}$	54
(87)	$CO_2^+ + CO_2 + M \rightarrow C_2O_4^+ + M$	$3.0 \times 10^{-28} \text{ cm}^6 \text{ s}^{-1}$	54
(88)	$O^+ + CO \rightarrow CO^+ + O$	$4.9 \times 10^{-12} \times (Tg/300)^{0.5} \times \exp[-4580/Tg] \text{ cm}^3 \text{ s}^{-1}$	57
(89)	$O^- + CO \rightarrow CO_2 + e^-$	$5.5 \times 10^{-10} \text{ cm}^3 \text{ s}^{-1}$	26
(90)	$CO_3^- + CO \rightarrow 2CO_2 + e^-$	$5 \times 10^{-13} \text{ cm}^3 \text{ s}^{-1}$	53
(91)	$C_2O_3^+ + CO \rightarrow CO_2 + C_2O_2^+$	$1.1 \times 10^{-9} \text{ cm}^3 \text{ s}^{-1}$	54
(92)	$C_2O_4^+ + CO \rightarrow C_2O_3^+ + CO_2$	$9.0 \times 10^{-10} \text{ cm}^3 \text{ s}^{-1}$	54
(93)	$C_2O_3^+ + CO + M \rightarrow C_2O_3^+ + CO_2 + M$	$2.6 \times 10^{-26} \text{ cm}^6 \text{ s}^{-1}$	54
(94)	$C_2O_4^+ + CO + M \rightarrow C_2O_3^+ + CO_2 + M$	$4.2 \times 10^{-26} \text{ cm}^6 \text{ s}^{-1}$	54
(95)	$C^+ + CO \rightarrow CO^+ + C$	$5.0 \times 10^{-13} \text{ cm}^3 \text{ s}^{-1}$	26
(96)	$CO^+ + C \rightarrow CO + C^+$	$1.1 \times 10^{-10} \text{ cm}^3 \text{ s}^{-1}$	57
(97)	$O_2^+ + C \rightarrow CO^+ + O$	$5.2 \times 10^{-11} \text{ cm}^3 \text{ s}^{-1}$	57
(98)	$O_2^+ + C \rightarrow C^+ + O_2$	$5.2 \times 10^{-11} \text{ cm}^3 \text{ s}^{-1}$	57
(99)	$C_2^+ + C \rightarrow C_2 + C^+$	$1.1 \times 10^{-10} \text{ cm}^3 \text{ s}^{-1}$	57
(100)	$O + CO_2^+ \rightarrow O_2^+ + CO$	$1.64 \times 10^{-10} \text{ cm}^3 \text{ s}^{-1}$	57
(101)	$O + CO_2^+ \rightarrow O^+ + CO_2$	$9.62 \times 10^{-11} \text{ cm}^3 \text{ s}^{-1}$	57
(102)	$O + CO_2^+ \rightarrow O_2^+ + CO_2$	$5.3 \times 10^{-11} \text{ cm}^3 \text{ s}^{-1}$	57
(103)	$CO_3^- + CO_2^+ \rightarrow 2CO_2 + O$	$5 \times 10^{-7} \text{ cm}^3 \text{ s}^{-1}$	53
(104)	$CO_4^- + CO_2^+ \rightarrow 2CO_2 + O_2$	$5 \times 10^{-7} \text{ cm}^3 \text{ s}^{-1}$	53
(105)	$CO_2^- + CO_2^+ \rightarrow CO + O_2 + O$	$6 \times 10^{-7} \text{ cm}^3 \text{ s}^{-1}$	53
(106)	$O + CO^+ \rightarrow CO + O$	$1.4 \times 10^{-10} \text{ cm}^3 \text{ s}^{-1}$	57
(107)	$O_2 + CO^+ \rightarrow O_2^+ + CO$	$1.2 \times 10^{-10} \text{ cm}^3 \text{ s}^{-1}$	57
(108)	$O_2 + C_2O_2^+ \rightarrow CO + CO + O_2^+$	$5.0 \times 10^{-12} \text{ cm}^3 \text{ s}^{-1}$	54
(109)	$C_2O_2^+ + M \rightarrow CO^+ + CO + M$	$1.0 \times 10^{-12} \text{ cm}^3 \text{ s}^{-1}$	54
(110)	$CO_3^- + C_2O_2^+ \rightarrow CO_2 + 2CO + O$	$5.0 \times 10^{-7} \text{ cm}^3 \text{ s}^{-1}$	54
(111)	$CO_4^- + C_2O_2^+ \rightarrow CO_2 + 2CO + O_2$	$5.0 \times 10^{-7} \text{ cm}^3 \text{ s}^{-1}$	54
(112)	$O_2^- + C_2O_2^+ \rightarrow 2CO + O_2$	$6.0 \times 10^{-7} \text{ cm}^3 \text{ s}^{-1}$	54
(113)	$CO_3^- + C_2O_3^+ \rightarrow 2CO_2 + CO + O$	$5.0 \times 10^{-7} \text{ cm}^3 \text{ s}^{-1}$	54
(114)	$CO_4^- + C_2O_3^+ \rightarrow 2CO_2 + CO + O_2$	$5.0 \times 10^{-7} \text{ cm}^3 \text{ s}^{-1}$	54
(115)	$O_2^- + C_2O_3^+ \rightarrow CO_2 + CO + O_2$	$6.0 \times 10^{-7} \text{ cm}^3 \text{ s}^{-1}$	54
(116)	$C_2O_4^+ + M \rightarrow CO_2^+ + CO_2 + M$	$1.0 \times 10^{-14} \text{ cm}^3 \text{ s}^{-1}$	54
(117)	$CO_3^- + C_2O_4^+ \rightarrow 3CO_2 + O$	$5.0 \times 10^{-7} \text{ cm}^3 \text{ s}^{-1}$	54
(118)	$CO_4^- + C_2O_4^+ \rightarrow 3CO_2 + O_2$	$5.0 \times 10^{-7} \text{ cm}^3 \text{ s}^{-1}$	54
(119)	$O_2^- + C_2O_4^+ \rightarrow 2CO_2 + O_2$	$6.0 \times 10^{-7} \text{ cm}^3 \text{ s}^{-1}$	54
(120)	$O_2^+ + CO_2^- \rightarrow CO_2 + O_2 + O$	$3 \times 10^{-7} \text{ cm}^3 \text{ s}^{-1}$	53

Table 8. continued

no.	reaction	rate coefficient	ref
(121)	$O + CO_3^- \rightarrow CO_2 + O_2^-$	$8 \times 10^{-11} \text{ cm}^3 \text{ s}^{-1}$	53
(122)	$O_2^+ + CO_4^- \rightarrow CO_2 + O_2 + O_2$	$3 \times 10^{-7} \text{ cm}^3 \text{ s}^{-1}$	53
(123)	$O + CO_4^- \rightarrow CO_3^- + O_2$	$1.1 \times 10^{-10} \text{ cm}^3 \text{ s}^{-1}$	26
(124)	$O + CO_4^- \rightarrow CO_2 + O_2 + O^-$	$1.4 \times 10^{-11} \text{ cm}^3 \text{ s}^{-1}$	26
(125)	$O + CO_4^- \rightarrow CO_2 + O_3^-$	$1.4 \times 10^{-11} \text{ cm}^3 \text{ s}^{-1}$	26
(126)	$O_3 + CO_4^- \rightarrow CO_2 + O_3^- + O_2$	$1.3 \times 10^{-10} \text{ cm}^3 \text{ s}^{-1}$	54
(127)	$O_2 + C^+ \rightarrow CO + O^+$	$6.2 \times 10^{-10} \text{ cm}^3 \text{ s}^{-1}$	57
(128)	$O_2 + C^+ \rightarrow CO^+ + O$	$3.8 \times 10^{-10} \text{ cm}^3 \text{ s}^{-1}$	26
(129)	$O^+ + O_2 \rightarrow O_2^+ + O$	$1.9e-11 \times (Tg(K)/300)^{-0.5} \text{ cm}^3 \text{ s}^{-1}$	26
(130)	$O_2^+ + O_2 + M \rightarrow O_4^+ + M$	$2.4 \times 10^{-30} \text{ cm}^6 \text{ s}^{-1}$	34
(131)	$O_2^- + O_2 + M \rightarrow O_4^- + M$	$3.5 \times 10^{-31} \text{ cm}^6 \text{ s}^{-1}$	34
(132)	$O^- + O_2 \rightarrow O_3 + e^-$	$1 \times 10^{-12} \text{ cm}^3 \text{ s}^{-1}$	54
(133)	$O^- + O_2 + M \rightarrow O_3^- + M$	$3.0 \times 10^{-28} \times (Tg(K)/300)^{-1} \text{ cm}^6 \text{ s}^{-1}$	54
(134)	$O^- + O_3 \rightarrow O_3^- + O$	$8 \times 10^{-10} \text{ cm}^3 \text{ s}^{-1}$	54
(135)	$O^- + O_3 \rightarrow O_2 + O_2 + e^-$	$3.0 \times 10^{-10} \text{ cm}^3 \text{ s}^{-1}$	58
(136)	$O_2^- + O_3 \rightarrow O_3^- + O_2$	$4.0 \times 10^{-10} \text{ cm}^3 \text{ s}^{-1}$	59
(137)	$O_3^- + O_3 \rightarrow O_2 + O_2 + O_2 + e^-$	$3.0 \times 10^{-10} \text{ cm}^3 \text{ s}^{-1}$	54
(138)	$O^+ + O_3 \rightarrow O_2^+ + O_2$	$1.0 \times 10^{-10} \text{ cm}^3 \text{ s}^{-1}$	34
(139)	$O^+ + O + M \rightarrow O_2^+ + M$	$1.0 \times 10^{-29} \text{ cm}^6 \text{ s}^{-1}$	59
(140)	$O^- + O \rightarrow O_2 + e^-$	$2.3 \times 10^{-10} \text{ cm}^3 \text{ s}^{-1}$	60
(141)	$O_2^- + O \rightarrow O_2 + O^-$	$3.3 \times 10^{-10} \text{ cm}^3 \text{ s}^{-1}$	59
(142)	$O_2^- + O \rightarrow O_3 + e^-$	$3.3 \times 10^{-10} \text{ cm}^3 \text{ s}^{-1}$	60
(143)	$O_3^- + O \rightarrow O_3 + O^-$	$1.0 \times 10^{-13} \text{ cm}^3 \text{ s}^{-1}$	58
(144)	$O_3^- + O \rightarrow O_2 + O_2 + e^-$	$1.0 \times 10^{-13} \text{ cm}^3 \text{ s}^{-1}$	54
(145)	$O_3^- + O \rightarrow O_2^- + O_2$	$2.5 \times 10^{-10} \text{ cm}^3 \text{ s}^{-1}$	54
(146)	$O_4^- + O \rightarrow O_3^- + O_2$	$4.0 \times 10^{-10} \text{ cm}^3 \text{ s}^{-1}$	34
(147)	$O_4^- + O \rightarrow O^- + O_2 + O_2$	$3.0 \times 10^{-10} \text{ cm}^3 \text{ s}^{-1}$	34
(148)	$O_4^- + O \rightarrow O_2^+ + O_3$	$3.0 \times 10^{-10} \text{ cm}^3 \text{ s}^{-1}$	34
(149)	$O^+ + O_2^- + M \rightarrow O_3 + M$	$2.0 \times 10^{-25} \text{ cm}^6 \text{ s}^{-1}$	59
(150)	$O^+ + O_2^- \rightarrow O + O_2$	$2.7 \times 10^{-7} \text{ cm}^3 \text{ s}^{-1}$	60
(151)	$O_2^+ + O_2^- \rightarrow O_2 + O_2$	$2.0 \times 10^{-7} \text{ cm}^3 \text{ s}^{-1}$	60
(152)	$O_2^+ + O_2^- \rightarrow O_2 + O + O$	$4.2 \times 10^{-7} \text{ cm}^3 \text{ s}^{-1}$	53
(153)	$O_2^+ + O_2^- + M \rightarrow O_2 + O_2 + M$	$2.0 \times 10^{-25} \text{ cm}^6 \text{ s}^{-1}$	59
(154)	$O_2^- + O_2 \rightarrow O_2 + O_2 + e^-$	$2.18 \times 10^{-18} \text{ cm}^3 \text{ s}^{-1}$	59
(155)	$O_2^- + M \rightarrow O_2 + M + e^-$	$2.7 \times 10^{-10} \times (Tg(K)/300)^{0.5} \times \exp(-5590/Tg(K)) \text{ cm}^3 \text{ s}^{-1}$	26
(156)	$O_2^+ + O_3^- \rightarrow O_2 + O_3$	$2.0 \times 10^{-7} \text{ cm}^3 \text{ s}^{-1}$	59
(157)	$O_2^+ + O_3^- \rightarrow O + O + O_3$	$1.0 \times 10^{-7} \text{ cm}^3 \text{ s}^{-1}$	59
(158)	$O^+ + O_3^- \rightarrow O_3 + O$	$1.0 \times 10^{-7} \text{ cm}^3 \text{ s}^{-1}$	59
(159)	$O_2 + O_3^- \rightarrow O_2 + O_3 + e^-$	$2.3 \times 10^{-11} \text{ cm}^3 \text{ s}^{-1}$	59
(160)	$O_3^- + M \rightarrow O_3 + e^-$	$2.3 \times 10^{-11} \text{ cm}^3 \text{ s}^{-1}$	26
(161)	$O^+ + O^- \rightarrow O + O$	$4.0 \times 10^{-8} \text{ cm}^3 \text{ s}^{-1}$	60
(162)	$O^+ + O^- + M \rightarrow O_2 + M$	$2.0 \times 10^{-25} \text{ cm}^6 \text{ s}^{-1}$	59
(163)	$O_2^+ + O^- \rightarrow O_2 + O$	$1.0 \times 10^{-7} \text{ cm}^3 \text{ s}^{-1}$	53
(164)	$O_2^+ + O^- \rightarrow O + O + O$	$2.6 \times 10^{-8} \text{ cm}^3 \text{ s}^{-1}$	60
(165)	$O_2^+ + O^- + M \rightarrow O_3 + M$	$2.0 \times 10^{-25} \text{ cm}^6 \text{ s}^{-1}$	59

Table 8. continued

no.	reaction	rate coefficient	ref
(166)	$M + O^- \rightarrow O + M + e^-$	$4 \times 10^{-12} \text{ cm}^3 \text{ s}^{-1}$	54
(167)	$M + O_4^- \rightarrow O_2^- + O_2 + M$	$3.08 \times 10^{-12} \text{ cm}^3 \text{ s}^{-1}$	58
(168)	$O_2^+ + M \rightarrow O_2^+ + O_2 + M$	$1.73 \times 10^{-13} \text{ cm}^3 \text{ s}^{-1}$	34

Table 9. Overview of the Vibrational Relaxation Processes upon Collision with Ground State Molecules, Included in the Model, Yielding Transformation to a Higher or Lower Vibrational Level (i.e., V–V Relaxations) or to the Ground State (i.e., V–T Relaxations), As Well As the Corresponding Rate Coefficients and References from Where These Data Were Adopted (EST Means Estimated)

no.	reaction	rate coefficient	ref	no.	reaction	rate coefficient	ref
(169)	$CO_2v1 + CO_2 \rightarrow CO_2 + CO_2$	$1.07 \times 10^{-14} \text{ cm}^3 \text{ s}^{-1}$	31	(188)	$CO_2v4 + CO_2 \rightarrow CO_2v2 + CO_2$	$4.33 \times 10^{-14} \text{ cm}^3 \text{ s}^{-1}$	31
(170)	$CO_2v1 + CO \rightarrow CO_2 + CO$	$7.48 \times 10^{-15} \text{ cm}^3 \text{ s}^{-1}$	31	(189)	$CO_2v4 + CO \rightarrow CO_2v2 + CO$	$3.03 \times 10^{-14} \text{ cm}^3 \text{ s}^{-1}$	31
(171)	$CO_2v1 + O_2 \rightarrow CO_2 + O_2$	$7.48 \times 10^{-15} \text{ cm}^3 \text{ s}^{-1}$	31	(190)	$CO_2v4 + O_2 \rightarrow CO_2v2 + O_2$	$3.03 \times 10^{-14} \text{ cm}^3 \text{ s}^{-1}$	31
(172)	$CO_2v2 + CO_2 \rightarrow CO_2 + CO_2$	$9.00 \times 10^{-18} \text{ cm}^3 \text{ s}^{-1}$	31	(191)	$CO_2v4 + O_2 \rightarrow CO_2v1 + CO_2$	$9.08 \times 10^{-18} \text{ cm}^3 \text{ s}^{-1}$	31
(173)	$CO_2v2 + CO \rightarrow CO_2 + CO$	$2.79 \times 10^{-17} \text{ cm}^3 \text{ s}^{-1}$	31	(192)	$CO_2v4 + CO \rightarrow CO_2v1 + CO$	$6.18 \times 10^{-15} \text{ cm}^3 \text{ s}^{-1}$	31
(174)	$CO_2v2 + O_2 \rightarrow CO_2 + O_2$	$2.79 \times 10^{-17} \text{ cm}^3 \text{ s}^{-1}$	31	(193)	$CO_2v4 + O_2 \rightarrow CO_2v1 + O_2$	$6.18 \times 10^{-15} \text{ cm}^3 \text{ s}^{-1}$	31
(175)	$CO_2v2 + CO_2 \rightarrow CO_2v1 + CO_2$	$2.90 \times 10^{-14} \text{ cm}^3 \text{ s}^{-1}$	31	(194)	$COv1 + CO_2 \rightarrow CO + CO_2$	$1.34 \times 10^{-23} \text{ cm}^3 \text{ s}^{-1}$	31
(176)	$CO_2v2 + CO \rightarrow CO_2v1 + CO$	$2.03 \times 10^{-14} \text{ cm}^3 \text{ s}^{-1}$	31	(195)	$COv1 + CO \rightarrow CO + CO$	$1.34 \times 10^{-23} \text{ cm}^3 \text{ s}^{-1}$	31
(177)	$CO_2v2 + O_2 \rightarrow CO_2v1 + O_2$	$2.03 \times 10^{-14} \text{ cm}^3 \text{ s}^{-1}$	31	(196)	$COv1 + O_2 \rightarrow CO + O_2$	$4.78 \times 10^{-24} \text{ cm}^3 \text{ s}^{-1}$	31
(178)	$CO_2v3 + CO_2 \rightarrow CO_2v2 + CO_2$	$7.72 \times 10^{-16} \text{ cm}^3 \text{ s}^{-1}$	31	(197)	$O_2v1 + CO_2 \rightarrow O_2 + CO_2$	$7.55 \times 10^{-23} \text{ cm}^3 \text{ s}^{-1}$	31
(179)	$CO_2v3 + CO_2 \rightarrow CO_2v2 + CO$	$2.32 \times 10^{-16} \text{ cm}^3 \text{ s}^{-1}$	31	(198)	$O_2v1 + CO \rightarrow O_2 + CO$	$2.52 \times 10^{-23} \text{ cm}^3 \text{ s}^{-1}$	31
(180)	$CO_2v3 + O_2 \rightarrow CO_2v2 + O_2$	$3.09 \times 10^{-16} \text{ cm}^3 \text{ s}^{-1}$	31	(199)	$O_2v1 + O_2 \rightarrow O_2 + O_2$	$2.52 \times 10^{-23} \text{ cm}^3 \text{ s}^{-1}$	31
(181)	$CO_2v3 + CO_2 \rightarrow CO_2v4 + CO_2$	$6.05 \times 10^{-15} \text{ cm}^3 \text{ s}^{-1}$	31	(200)	$O_2v2 + CO_2 \rightarrow O_2 + CO_2$	$7.55 \times 10^{-23} \text{ cm}^3 \text{ s}^{-1}$	EST ³²
(182)	$CO_2v3 + CO \rightarrow CO_2v4 + CO$	$1.81 \times 10^{-15} \text{ cm}^3 \text{ s}^{-1}$	31	(201)	$O_2v2 + CO \rightarrow O_2 + CO_2$	$2.52 \times 10^{-23} \text{ cm}^3 \text{ s}^{-1}$	EST ³²
(183)	$CO_2v3 + O_2 \rightarrow CO_2v4 + O_2$	$2.42 \times 10^{-15} \text{ cm}^3 \text{ s}^{-1}$	31	(202)	$O_2v2 + O_2 \rightarrow O_2 + O_2$	$2.52 \times 10^{-23} \text{ cm}^3 \text{ s}^{-1}$	EST ³²
(184)	$CO_2v3 + CO_2 \rightarrow CO_2v1 + CO_2v2$	$2.42 \times 10^{-15} \text{ cm}^3 \text{ s}^{-1}$	31	(203)	$O_2v3 + CO_2 \rightarrow O_2 + CO_2$	$7.55 \times 10^{-23} \text{ cm}^3 \text{ s}^{-1}$	EST ³²
(185)	$CO_2v3 + CO_2 \rightarrow CO_2v1 + CO_2$	$1.70 \times 10^{-18} \text{ cm}^3 \text{ s}^{-1}$	31	(204)	$O_2v3 + CO \rightarrow O_2 + CO$	$2.52 \times 10^{-23} \text{ cm}^3 \text{ s}^{-1}$	EST ³²
(186)	$CO_2v3 + CO \rightarrow CO_2v1 + CO$	$5.10 \times 10^{-19} \text{ cm}^3 \text{ s}^{-1}$	31	(205)	$O_2v3 + O_2 \rightarrow O_2 + O_2$	$2.52 \times 10^{-23} \text{ cm}^3 \text{ s}^{-1}$	EST ³²
(187)	$CO_2v3 + O_2 \rightarrow CO_2v1 + O_2$	$6.80 \times 10^{-19} \text{ cm}^3 \text{ s}^{-1}$	31				

model. Also, the vibrational kinetics for CO_2 might in reality be more complex, because higher vibrational levels might be important, although we expect this to be limited in a DBD plasma. When applying the model to a microwave plasma or a gliding arc plasma, the vibrational kinetics scheme should be extended to the higher vibrational levels.

The densities and rates of the important reactions of the different plasma species (i.e., electrons, vibrationally excited CO_2 molecules, various neutrals and ions) are plotted as a function of time during one pulse and afterglow, as well as for five consecutive pulses with an interpulse period of 1 μs , to mimic the filamentary behavior of a DBD. The production rates of vibrationally and electronic excited CO_2 were found to be at least 2 orders of magnitude higher than the other electron impact reaction rates, i.e., dissociation, ionization, dissociative ionization, and attachment. As a result, the densities of the vibrationally excited species were found to be only 2 orders of magnitude lower than the ground state CO_2 density, during the pulse. We have also pointed out the effect of accumulation on the density of vibrationally excited CO_2 . The accumulation was found to be significant at interpulse times below 1 μs , but at an interpulse time between 1 and 10 μs the vibrationally excited CO_2 molecules start to fall back to the ground state, and above an interpulse time of 10 microseconds most of the vibrationally excited CO_2 molecules have decayed back into the ground state. The interpulse time between two filaments is not

exactly known in a DBD, but our results indicate that it could be possible that locally the density of vibrationally excited CO_2 molecules, and hence their role in the CO_2 splitting, increases as a result of accumulation due to successive filaments.

The neutrals of interest were found to be molecular oxygen and CO, which are also reported in literature as the dominant end products.^{2,3,7} The role of neutrals in the CO_2 splitting was, however, not found to be significant, although atomic oxygen seems to play a vital role in the formation of molecular oxygen and ozone. We also investigated the role of the ions in the plasma and identified short living ions which are formed and lost during the 30 ns pulse, as well as long living ions which have a significant density even in the millisecond range.

We can summarize our findings regarding the net contribution of the different plasma species and reactions to the dissociation of CO_2 as follows:

1. The splitting of ground state CO_2 is dominated by electron impact reactions, and predominantly by electron impact dissociation. Electron impact ionization is also important but is compensated by the fact that a large fraction of the formed ions will eventually recombine, resulting again in the formation of CO_2 .
2. The splitting of vibrationally excited CO_2 is mainly dominated by ion reactions, followed by electron impact dissociation.

3. 94% of the CO₂ splitting is achieved from the ground state, whereas 6% occurs from the vibrationally excited states. This contribution is, however, calculated for one pulse and a long afterglow. If the interpulse period between two successive filaments is shorter, accumulation effects can occur for the vibrationally excited molecules, and consequently, their role can be (much) higher.

In future work, this model will be used for long time-scale simulations, matching the residence time of real gas conversion in DBDs, to obtain information on the splitting efficiency, both in terms of conversion and energy efficiency, as well as the selectivities and yields of the reaction products.

■ APPENDIX

Tables 5–9 with the chemical reactions included in the model.

■ AUTHOR INFORMATION

Corresponding Author

*E-mail: robby.aerts@ua.ac.be.

Notes

The authors declare no competing financial interest.

■ ACKNOWLEDGMENTS

We are very grateful to M. Kushner and group members for providing the global_kin code and for the useful advice. This work was carried out using the Turing HPC infrastructure at the CalcUA core facility of the Universiteit Antwerpen, a division of the Flemish Supercomputer Center VSC, funded by the Hercules Foundation, the Flemish Government (department EW1) and the Universiteit Antwerpen.

■ REFERENCES

- (1) Zhou, L. M.; Xue, B.; Kogelschatz, U.; Eliasson, B. *Energ. Fuel* **1998**, *12*, 1191–1199.
- (2) Indarto, A.; Choi, J.-W.; Lee, H.; Song, H. K. *Environ. Eng. Sci.* **2012**, *23*, 1033–1043.
- (3) Paulussen, S.; Verheyde, B.; Tu, X.; De Bie, C.; Martens, T.; Petrovic, D.; Bogaerts, A.; Sels, B. *Plasma Sources Sci. Technol.* **2010**, *19*, 034015.
- (4) Sherif, S. A.; Barbir, F.; Veziroglu, T. N. *SoEn* **2005**, *78*, 647–660.
- (5) Yang, H.; Xu, Z.; Fan, M.; Gupta, R.; Slimane, R. B.; Bland, A. E.; Wright, I. J. *Environ. Sci. (China)* **2008**, *20*, 14–27.
- (6) Matsumoto, H.; Tanabe, S.; Okitsu, K.; Hayashi, Y.; Suib, S. L. *Bull. Chem. Soc. Jpn.* **1999**, *72*, 2567–2571.
- (7) Spencer, L. F.; Gallimore, A. D. *Plasma Chem. Plasma P.* **2010**, *31*, 79–89.
- (8) Indarto, A.; Yang, D. R.; Choi, J.-W.; Lee, H.; Song, H. K. *J. Hazard. Mater.* **2007**, *146*, 309–15.
- (9) Hokazono, H.; Obara, M.; Midorikawa, K.; Tashiro, H. *J. Appl. Phys.* **1991**, *69*, 6850.
- (10) Fridman, A. *Plasma Chemistry*; Cambridge University Press: New York, 2008.
- (11) Fridman, A.; Rusanov, V. D. *Pure Appl. Chem.* **1994**, *66*, 1267–1278.
- (12) Semiokhin, I. A.; Andreev, Y. P.; Panchenkov, G. M. *Russ. J. Phys. Chem.* **1964**, *38*, 1126–1128.
- (13) Andreev, Y. P.; Semiokhin, I. A.; Panchenkov, G. M.; Baraev, V. V. *Russ. J. Phys. Chem.* **1964**, *38*, 431–434.
- (14) Semiokhin, I. A.; Andreev, Y. P. *Russ. J. Phys. Chem.* **1966**, *40*, 1279–1282.
- (15) Luk'yanov, V. B.; Emel'yanov, Y. M.; Aleksandrova, I. F. *Russ. J. Phys. Chem.* **1967**, *41*, 86–90.
- (16) Luk'yanov, V. B.; Emel'yanov, Y. M.; Kovalenko, V. V. *Russ. J. Phys. Chem.* **1967**, *41*, 1081–1083.
- (17) Luk'yanov, V. B. *Russ. J. Phys. Chem.* **1967**, *41*, 1083–1085.
- (18) Luk'yanov, V. B.; Nesmeyanov, A. N.; Bachinin, V. G. *Russ. J. Phys. Chem.* **1967**, *41*, 1438–1441.
- (19) Luk'yanov, V. B. *Russ. J. Phys. Chem.* **1967**, *41*, 1536–1537.
- (20) Luk'yanov, V. B.; Simonov, E. F.; Golovanov, V. I. *Russ. J. Phys. Chem. J. Phys. Chem.* **1969**, *43*, 640–645.
- (21) Siemens, W. *Ann. Phys.* **1857**, *178*, 66–122.
- (22) Eliasson, B.; Kogelschatz, U. *IEEE Trans. Plasma Sci.* **1991**, *19*, 309–323.
- (23) Dorai, R. Modeling of Atmospheric Pressure Plasma Processing of Gases and Surfaces. Ph.D. Thesis; University of Illinois: Urbana-Champaign, 2002.
- (24) Dorai, R.; Kushner, M. J.; Hassouni, K. *J. Appl. Phys.* **2000**, *88*, 6060.
- (25) Lowke, J. J.; Phelps, A.; Irwin, B. W. *J. Appl. Phys.* **1973**, *44*, 4664.
- (26) Beuthe, T. G.; Chang, J.-S. *J. Appl. Phys.* **1997**, *36*, 4997–5002.
- (27) Jain, A.; Norcross, D. *Phys. Rev. A* **1992**, *45*, 1644–1656.
- (28) Liu, W.; Victor, G. A. *ApJ* **1994**, *435*, 909.
- (29) Phelps, A. V. *Tabulations of collision cross sections and calculated transport and reaction coefficients for electron collisions with O₂* Technical Report 28, JILA information center (1985)
- (30) Raju, G. G. *Gaseous Electronics: Theory and Practice*; CRC Press: Boca Raton, FL, 2011; DOI: 10.1201/9780203025260.
- (31) Blauer, J. A.; Nickerson, G. R. *A survey of vibrational relaxation rate data for processes important to CO₂-N₂-H₂O infrared plume radiation* Technical Report AFRPL-TR-73-57, ULTRASYSTEMS, Irvine, 1973.
- (32) Surzhikov, S. T. *Non-Equilibrium Gas Dynamics – From Physical Models to Hypersonic Flights*; Moscow, 2009; p 948.
- (33) Chirokov, A.; Gutsol, A.; Fridman, A. *Pure Appl. Chem.* **2005**, *77*, 487–495.
- (34) A. Kossyi, I.; Yu Kostinsky, A.; A. Matveyev, A.; V. Silakov, P. *Plasma Sources Sci. Technol.* **1992**, *1*, 207–220.
- (35) Cenian, A.; Chernukho, A.; Borodin, V.; Śliwiński, G. *Contrib. Plasma Phys.* **1994**, *34*, 25–37.
- (36) Tu, X.; Gallon, H. J.; Twigg, M. V.; Gorry, P. A.; Whitehead, J. C. J. *Phys. D Appl. Phys.* **2011**, *44*, 274007.
- (37) Kogelschatz, U. In *HAKONE VII Int. Symp. On High Pressure Low*; 2000.
- (38) Slovetsky, D. I. Kinetics and Mechanisms of Physical and Chemical Processes in Non-Equilibrium Plasma-Chemical Systems, Ph.D. Thesis, USSR Academy of Sciences: Moscow, 1979.
- (39) Gutsol, A.; Rabinovich, A.; Fridman, A. *J. Phys. D Appl. Phys.* **2011**, *44*, 274001.
- (40) Rabinovich A.; Nunnally T.; Fridman A., (Drexel University, USA). Non-equilibrium gliding arc plasma system for CO₂ dissociation. US Patent 2012/0090985 A1, October 3, 2011.
- (41) Savinov, S. Y.; Lee, H.; Song, H. K.; Na, B.-K. *Korean J. Chem. Eng.* **2002**, *19*, 564–566.
- (42) Nunnally, T.; Gutsol, K.; Rabinovich, A.; Fridman, A.; Gutsol, A.; Kemoun, A. *J. Phys. D Appl. Phys.* **2011**, *44*, 274009.
- (43) Bulos, B.; Phelps, A. *Phys. Rev. A* **1976**, *14*, 615–629.
- (44) Amouroux, J.; Cavadias, S.; Doubla, A. *IOP Conf. Ser.: Mater. Sci. Eng.* **2011**, *19*, 012005.
- (45) Janev, R. K.; Reiter, D. *ChemInform* **2003**, *34*.
- (46) Janev, R. K.; Wang, J. G.; Murakami, I.; Kato, T. *Cross sections and rate coefficients for electron-impact ionization of hydrocarbon molecules* Research Report; Tokio, Japan, 2001.
- (47) Krishnakumar, E.; Srivastava, S. K. *Int. J. Mass Spectrom. Ion Processes* **1992**, *113*, 1–12.
- (48) Liu, C.; Eliasson, B.; Xue, B.; Li, Y.; Wang, Y. *React. Kinet. Catal. Lett.* **2001**, *74*, 71–77.
- (49) Eliasson, B.; Kogelschatz, U. Basic data for modelling of electrical discharges in gases: oxygen. *Brown Boveri Research Report KLR 86-11C* **1986**, *1*–148.
- (50) Matejčík, S.; Kiendler, A.; Cicman, P.; Skalný, J.; Stampfli, P.; Illenberger, E.; Chu, Y.; Stamatovic, A.; Märk, T. D. *Plasma Sources Sci. Technol.* **1997**, *6*, 140–146.
- (51) Itikawa, Y.; Ichimura, A. *J. Phys. Chem. Ref. Data* **1990**, *19*, 637.
- (52) Laher, R. R.; Gilmore, F. R. *J. Phys. Chem. Ref. Data* **1990**, *19*, 277.
- (53) Hokazono, H.; Fujimoto, H. *J. Appl. Phys.* **1987**, *62*, 1585.

- (54) Cenian, A.; Chernukho, A.; Borodin, V. *Contrib. Plasm Phys.* **1995**, *35*, 273–296.
- (55) Eliasson, B.; Hirth, M.; Kogelschatz, U. *J. Phys. D Appl. Phys.* **1987**, *20*, 1421–1437.
- (56) Hadj-Ziane, S.; Held, B.; Pignolet, P.; Peyrous, R.; Coste, C. *J. Phys. D Appl. Phys.* **1992**, *25*, 677–685.
- (57) Woodall, J.; Agúndez, M.; Markwick-Kemper, A. J.; Millar, T. J. *Astron. Astrophys.* **2007**, *466*, 1197–1204.
- (58) Ionin, A. A.; Kochetov, I. V.; Napartovich, A. P.; Yuryshev, N. N. *J. Phys. D Appl. Phys.* **2007**, *40*, R25–R61.
- (59) Eliasson, B.; Hirth, M.; Kogelschatz, U. *J. Phys. D Appl. Phys.* **1987**, *20*, 1421–1437.
- (60) Gudmundsson, J. T.; Thorsteinsson, E. G. *Plasma Sources Sci. Technol.* **2007**, *16*, 399–412.